Rheological, Structural and Melt Spinnability Study on Thermoplastic Starch/PLA Blend Biopolymers and Tensile, Thermal and Structural Characteristics of Melt Spun Fibers

Selamu Temesgen[1,2,3,*], Lucas Großmann[1], Tamrat Tesfaye[2], Ines Kuehnert[4], Norbert Smolka[4] and Michael Nase[1]

[1]*Institute for Circular Economy of Bio: Polymers at Hof University (ibp), 95028 Hof/Saale, Germany*

[2]*Ethiopian Institute of Textile and Fashion Technology, Bahir Dar University, Bahir Dar P.O. Box 1037, Ethiopia*

[3]*School of Textiles, Kombolcha Institute of Technology, Wollo University, Kombolcha P.O. Box 208, Ethiopia*

[4]*Leibniz-Institut fuer Polymerforschung Dresden e.V., Hohe Str. 6, D-01069 Dresden, German*

Abstract: In this study, rheology, structure and melt spinnability of thermoplastic starch TPS/PLA blend compounds as well as characteristics of melt spun fibers was studied. Thermoplastic starch is further modified with tartaric acid and blends are compatibilized using graft copolymer, maleic anhydride grafted PLA. Results from rheology analysis of compounds shows significantly reduced melt flow rate MFR and reduced viscosity as a result of tartaric acid modification and compatibilization, but the viscosity was increased as TPS_TA content in the blend increased. In addition, storage modulus (G`) and loss modulus (G``) were increased with increasing TPS_TA content in the blends. Fourier transform infrared spectroscopy FTIR analysis confirmed O-H peak shifts and peak intensity changes associated to starch thermosplasticization and further peak shifts associated with more O-H bond breakages due to tartaric acid modification, indicating acid hydrolysis action of tartaric acid which agrees with results from rheology study. Melt spinning trials show the possibility of melt spinning of biopolymer fibers from blends with up to 40%w/w TPS_TA content. The melt spun fibers have diameter in range of 12.0–124.0 µm depending on take up speed and TPS_TA content. Differential scanning calorimetry DSC analysis of melt spun fibers shows glass transition T_g shifts attributed to molecular orientation and rigid amorphous TPS phase formation as well as the occurrence of double melting peaks T_m associated to different crystals resulting from induced crystallization. The overall result from this study shows the possibility of melt spinning thermoplastic starch/PLA blend biopolymers in to fibers, revealing opportunity to utilize starch biopolymer for fiber spinning. Furthermore, the results also show the need for further research engagements to get fibers with better performance.

Keywords: Thermoplastic starch, biopolymer, sustainable polymer, melt spinning, tartaric acid, shear viscosity.

1. INTRODUCTION

Addressing the challenges of plastics production from petroleum based feed stock has become a priority for major global entities, including the United Nations Environment Assembly Programme (UNEA-5.2), World Economic Forum (WEF), the World Health Organization, and the European Union (EU) [1].

The development of bio-based and biodegradable plastics as an alternative to petroleum-based polymers has emerged as a topic of interest for creating future materials capable of various sustainable applications. Different sectors within the plastics industry, including the fiber and textile sector, are striving to engage in this green transition. Global fiber production reached 111 million metric tons, having doubled over the past 20 years [2]. However, the synthetic fibers of petrochemical origin dominate the current global textile market, among them polyethylene terephthalate (PET) with a global market share of 52% in 2020 [2, 3].

More recently, the textile industry has embraced the adoption of bio-based and biodegradable polymers, with the textile market projected to grow at a compound average growth rate (CAGR) of 12% over the next decade, the aim is to reduce the negative environmental impact of petrochemical polymers [1, 4]. Biodegradable polymer fibers with added functionalities are in high demand for various applications, including biomedicine, textiles, and others [6-8]. A wide range of biodegradable polymers derived from both synthetic and natural sources exist, but many of them suffer from processing difficulties and high cost.

Some of the common biodegradable thermoplastics produced at industrial scale include polylactic acid (PLA), polyhydroxyalkanoates (PHAs), thermoplastic starch (TPS), polybutylene adipate terephthalate (PBAT), polybutylene succinate (PBS), and polycaprolactone (PCL) [1, 5] among others.

*Address corresponding to this author at the Institute for Circular Economy of Bio: Polymers at Hof University (ibp), 95028 Hof/Saale, Germany;
E-mail: peace.tem@gmail.com, stemesgen@hof-university.de

E-ISSN: 1929-5995/24

Starch is an abundant biopolymer with potential use as a sustainable substitute for petrochemical polymers in the textile and plastics industry as well as other industrial applications [10]. The manufacture of materials based on starch represents an important potential in the market due to the wide availability of its raw material, biodegradability, low cost and the versatility for making chemical modifications [11].

Native starch does not exhibit a good processability. Therefore starch needs modifications to be used in industrial applications [12]. Thermal modification of starch can be done by thermo-plasticization, intended to convert it into a thermoplastic material in the presence of plasticizer, heat and shear force, by de-structuring the granular structure of starch crystallites. The efficiency of starch thermoplasticization depends on the capacity for hydrogen bonding and cleaving of the starch chains. In this sense, the loss of crystallinity is responsible for the de-structuring of the starch granules, thereby affecting the material stability and the physical-mechanical properties [13]. Nevertheless, thermoplastic starch has drawbacks, such as poor mechanical properties, very high hydrophilicity, high viscosity and poor thermal stability [12, 13].

Combination with existing biodegradable polymers to create new biodegradable or functional materials became an effective strategy to produce materials with comparable properties [14, 15]. PLA, a biodegradable polymer, has received great attention due to its advanced applications, versatility, and properties [17, 18]. However, due to its high cost and brittle nature as compared to non-degradable polymers, its application is limited [20]. Blends of PLA and TPS have been developed to overcome the low degradation rate and high cost of PLA and improve the performance and functionality of TPS. According to Mayekar *et al*. 2023, TPS can accelerate the biodegradation of PLA in industrial composting conditions and in home composting settings [21]. Despite these benefits, both biopolymers are thermodynamically immiscible and present poor interfacial adhesion, making it difficult to achieve favorable processing and performance properties [22]. In the recent years numerous studies investigated the possibilities of introducing different reactive coupling agents in order to enhance the interfacial adhesion between TPS and PLA, among which, the use of reactive compatibilizers is most common [19-22]. The compatibilization of polymeric materials from different sources has been used more often to achieve adequate synergy and guarantee the best properties in the product [15, 23].

Usually TPS has a high molecular weight and complex structure to achieve the viscosity and melt extensibility required to prevent fracture and failure of the fibers as they are formed when it is blended with other biopolymers [18]. Hence besides thermoplas-ticization and blending, further modification of the properties of thermoplastic starch and improving its miscibility with other biopolymers is required to better utilize this abundant biopolymer for textile applications [28].

Among the different starch modification methods, chemical modification can be a strategy to overcome the drawbacks and increase its processability by reducing the viscosity, weakening the intermolecular hydrogen bonds, and decreasing the molecular weight [26, 29]. The chemical modification of native starch causes structural changes in the polymer molecule affecting their physio-chemical properties which make them suitable for industrial uses. Acid hydrolysis is an important chemical modification that can significantly change the structural and functional properties of starch without disrupting its granular morphology [31]. Different organic acids have been used by previous researchers to modify the properties of starch [15, 20]. However, based on a literature survey, there is no research report focused on starch modification with tartaric acid combined with thermoplasticization, and studying its melt spinnability (eco-friendly and scalable fiber spinning method) by blending with other biopolymers. Hence, this study aims for melt spinning of TPS based biopolymer compounds by modifying the properties of native starch and studying the properties of melt spun fibers.

2. EXPERIMENTAL

2.1. Materials

Tapioca starch from SWI.Co.TH, Thailand with a moisture content of 11.6% was supplied by Ferdinand Kreutzer-Sabamühle, Germany. PLA Luminy® LX530 a medium flow fiber-grade resin with (98% L-isomer content, density of 1.24 g/cm^3 and melt flow index of 23 g/10 min) was purchased from (Total Corbion). Industrial grade glycerol of 99.5 % purity having a molecular weight 92.04 g/ml was purchased from (chemiekontor.de GmbH). Tartaric acid, having a molecular weight of 150.09 g/mol and a density of 1.79 g/ml in form of a crystallin powder was supplied by (Algin Chemie e.K, Germany). Maleic anhydride, in white large crystals (chunks) with a purity of 98.5 % and molecular weight of 98.06 g/mol was purchased

from Sigma Aldrich and dicumyl peroxide of 98 % purity, a white crystallin powder with a molecular weight of 270.37 g/mol, was also purchased from Sigma Aldrich.

2.2. Preparation of Thermoplastic Starch (TPS) and TPS_TA

Conversion of native starch into thermoplastic material was done using a co-rotating twin screw extruder available at the Institute for Circular Economy of Bio:Polymers at Hof University (ibp), Germany. Starch melt extrusion was done in two phases: the first phase without tartaric acid and the second phase with the addition of tartaric acid. To convert starch into thermoplastic material, 30%w/w (starch dry mass basis) glycerol was used as a plasticizer in the first phase of TPS preparation. In the second phase, starch, glycerol (30 %w/w starch mass basis) and tartaric acid with a content of 0.5 %w/w (based on starch mass), as an additive to improve the viscosity of TPS, was used.

Starch powder and the predetermined amount of tartaric acid in powder form were dry mixed and glycerol was added and mixed for about 1 hour at medium speed in a kitchen mixer (BOSCH MUM4, Germany). The melt extrusion was done on a co-rotating twin screw extruder (Lab Tech Engineering Co., Ltd, Thailand) with a screw length to diameter ratio (L/D) of 44 and a screw diameter of 20 mm.

The pre-mixed starch, glycerol and tartaric acid (TA) mixture was fed into the hopper of the twin screw extruder and melt extruded into thermoplastic starch (TPS) strands. The melt extruded strands were air cooled; cut and pelletized using the inline granulator and the TPS granulates were collected for further study. Extrusion parameters and material proportions for TPS extrusion are given in Table **1**.

2.3. Preparation of Compatibilizer - Maleic Anhydride Grafted PLA (PLA-g-MA)

The grafting of PLA takes place by reactive extrusion of PLA and maleic anhydride in the presence of dicumyl peroxide (DCP) as an initiator, on a co-rotating twin screw extruder. Prior to grafting, PLA granulate was dried for 8 hours at 70 °C using a LUXOR CAS compressed air dryer (Motan Holding GmbH, Konstanz, Germany). The maleic anhydride (2 %w/w based on PLA mass) and 0.75 %w/w of DCP as an initiator were premixed in a corrosion resistant container and then fed into the hopper of the co-rotating twin screw extruder for melt extrusion. The melt extruded strands were pelletized/granulated and the granules were collected to be used as com-patibilizer during TPS/PLA blend preparation. Process parameters and material proportions for PLA-g-MA preparation are given in Table **2**.

Maleic anhydride (MA) grafting onto the PLA backbone takes place through free radical reaction with two possible mechanisms. In the first mechanism (path A), the DCP initiator converts PLA into a macro-radical by extracting hydrogen from the PLA structure. This macro-radical provides a site for grafting MA onto the PLA. In the alternate mechanism (path B), presence of the radical initiator, not only extracts hydrogen from PLA but also results in β-chain scission of the polymer reducing molecular weight. Figure **1** shows the possible mechanisms of reaction between PLA and MA.

Table 1: Extrusion Parameters for TPS Preparation

Sample name	Starch (%w/w)	Glycerol (%w/w)	Tartaric acid (%w/w)	Screw speed (rpm)	Feed rate Kg/h
Neat TPS	70	30	-	120	2
TPS_TA	70	30	0.5	120	2
Extrusion temperature for TPS preparation					
Temperature (°C)	Feed-100 /110/110/120/120/130/130/130/130125/125 -Die				

Table 2: Process Parameters and Material Proportions for PLA-g-MA Preparation

Sample name	PLA (%w/w)	MA (%w/w)	DCP (%w/w)	Screw speed (rpm)	Feed rate Kg/h
PLA-g-MA	98	2	0.75	80	2
Extrusion temperature for graft compounding					
Temperature (°C)	Feed-155 /160/165/165/170/180/180/180/175/175/170 -Die				

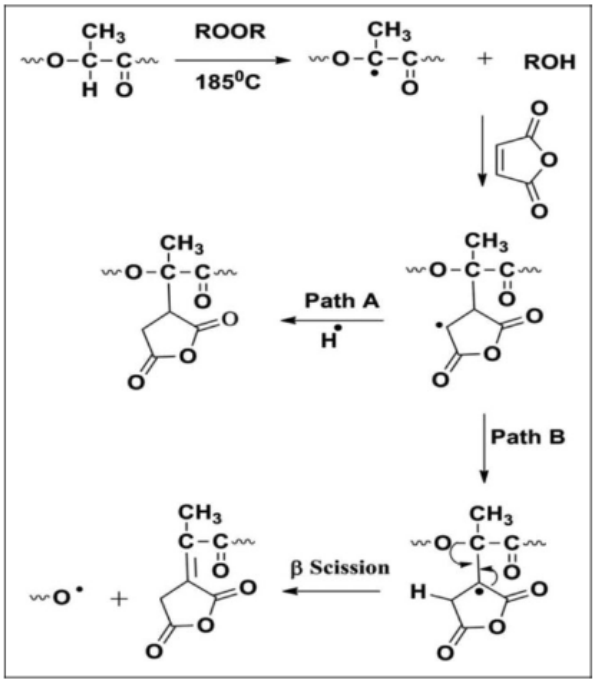

Figure 1: Proposed mechanisms of MA grafting onto the PLA backbone [33].

2.4. Preparation of Polymer Blend Compounds

The melt extruded TPS, TPS_TA and PLA granulates were melt blended in the presence of PLA-g-MA as a compatibilizer using a co-rotating twin screw extruder with a screw length to diameter ratio (L/D) of 44 and screw diameter of 20 mm. Prior to melt extrusion TPS, PLA and PLA-g-MA granulates were each dried for 8 hours at 70 °C by using a LUXOR CAS compressed air dryer (Motan Holding GmbH, Konstanz, Germany).

Then the dried granulates were physically mixed based on the predetermined composition for each blend compound and fed into the hopper of the extruder. The parameters for melt extrusion and blend proportions are given in Table **3**.

2.5. Melt Spinning

Melt spinning of the TPS_TA based blend compounds was done on the mono filament piston type melt spinning device available at Leibniz-Institut für Polymerforschung e.V. (Dresden), Germany. The piston type melt spinning device has a single barrel piston and is equipped with a capillary hole of 0.3 mm diameter (D), the ratio of the capillary length L to the capillary diameter (L/D) being 2. The pre-dried (for 12 hours at 40 °C) polymer samples were filled in and melted at 180 °C. Subsequently, the molten material was forced by a piston through a single hole die. A winder was used to collect the melt as spun monofilaments with varying take-up speeds with the intention of finding the maximum spinnable take-up speed for each compound.

Compatibilized compounds that were prepared with tartaric acid addition were selected for melt spinnability testing on the standard device, due to their better performance in preliminary tests done on another non-standard simple device used for filament spinning.

Table 3: Process Parameters and Blend Proportion for the Preparation of Blend Compounds

Compound name	TPS (%w/w)	TPS_TA (%w/w)	PLA (%w/w)	PLA-g-MA (%w/w)	Screw speed (rpm)	Feed rate Kg/h
40TPS/60PLA	40	-	60	-	120	2
40TPS_TA/60PLA	-	40	60	-	120	2
40TPS/48PLA12PLA-g-MA	40	-	48	12	120	2
40TPS_TA/48PLA/12PLA-g-MA		40	48	12	120	2
30TPS/70PLA	30	-	70	-	120	2
30TPS_TA/70PLA	-	30	70	-	120	2
30TPS/56PLA/14PLA-g-MA	30	-	56	14	120	2
30TPS_TA/56PLA/14PLA-g-MA		30	56	14	120	2
10TPS/90PLA	10	-	90	-	120	2
10TPS_TA/90PLA	-	10	90	-	120	2
10TPS/72/PLA18PLA-g-MA	10	-	72	18	120	2
10TPS_TA/72PLA/18PLA-g-MA	-	10	72	18	120	2
Neat PLA		-	100	-	-	-
Extruded PLA	-	-	100	-	120	2
Extrusion temperature for blend compounding						
Temperature (°C)	Feed-135/150/160/160/163/170/170/170/165/160/155 -Die					

The material composition, parameters for melt spinning and melt spun fiber diameter measurements are given in Table **4** in the results section.

3. BASIC CHARACTERIZATIONS

3.1. Rheology Study

The rheology study was done with the direct flow method using a melt flow index device and with a rotational rheometer.

3.1.1. Melt Flow Index Measurement

Melt flow index (MFI) or melt flow rate (MFR) is a measure of a given polymers' flow characteristics also known as the rheological property in the molten state under a known pressure and temperature. Ergo, it is a measure of the ease of flow of a thermoplastic polymer melt. It can also be defined as the weight of polymer in grams flowing in 10 min (g/10min) through a die of a specific diameter with application of pressure by a defined weight at a given temperature.

The MFI measurement in this study was conducted on a Karg Industrietechnik MFI device following the ISO 1133 standard test method using an applied load of 2.16 kg and a temperature of 180 °C with a pre-heating time of 300 s.

3.1.2. Rheological Measurement using Rotational Rheometer

To measure the rheological properties of the prepared polymer compounds, a rotational rheometer Discovery HR-2 hybrid from TA instruments was used. The plate-plate geometry with a diameter of 25 mm and a gap of 10 mm was used to conduct measurements under air atmosphere. The steady shear flow measurements at different temperatures were conducted using a shear rate ranging from 0.1 – 100 /s. The dynamic oscillatory frequency sweep test was performed at a constant strain of 1 % and a frequency ranging from 100 HZ–0.1 HZ at various temperatures.

3.2. Thermal Characterization

Thermal characterization of the melt spun fibers was done using the differential scanning calorimetry DSC 214 Polyma instrument (NETZSCH-Gerätebau GmbH). The DSC analysis was conducted to find out the thermal transitions and crystallinity behavior of the fibers as a result of different take-up speeds.

For DSC measurement, a fiber sample mass of 6.5 – 8.5 mg was used in a nitrogen gas atmosphere with a gas flow rate of 40 ml/min. The samples were heated at a constant heating rate of 10 K/min within a temperature range of -20 °C to 200 °C for the first heating cycle followed by a cooling cycle from 200 °C to -20 °C and a second heating cycle from -20 °C to 200 °C.

The thermal characteristics of the melt spun fibers were analyzed to see the effect of take-up speed on thermal transitions. The percent crystallinity of the polymer was calculated using the heat of melting (ΔH_m) and the heat of cold crystallization (ΔH_c) according to the following equation:

$$\% \ crystallinity = \frac{\Delta Hm - \Delta Hc}{\Delta Hm^{\circ} \times wf} \times 100\% \quad (1)$$

Where ΔHm° is the theoretical heat of melting for 100% crystalline PLA which is (93 J/g) [34] and W*f* is the weight fraction of PLA in the blend.

3.3. Structural Characterization

3.3.1. Fourier Transform Infrared Spectroscopy (FTIR) Characterization

The structural characterization of polymer compounds was performed using fourier transform infrared spectroscopy (FTIR). In FTIR spectra, most molecules absorb light in the infrared region of the electromagnetic spectrum, converting it to molecular vibration. This absorption is characteristic for the nature of the chemical bonds present in a sample.

In this study FTIR analysis was performed in ATR (attenuated total reflection) modality on polymer pellets and the ATR spectra were recorded using a Bruker Tensor 27 FT-IR spectrometer (Bruker optic, Germany). The samples were heated from 30 °C to 250 °C, with increments of 10 °C, and the spectra were recorded every 10 °C at wave numbers ranging from 400 cm^{-1} to 4000 cm^{-1}.

3.4. Tensile Test for Melt Spun Fibers

In this study, a Zwick Roell tensile testing device was used to carry out tensile test measurements of melt spun fiber samples using a clamping distance of 200 mm. Prior to tensile testing, the samples were conditioned for 24 hours at 50% relative humidity and 22 °C to minimize the environmental effect on the fiber properties.

3.5. Fiber Surface Morphology

3.5.1. Microscopic Images of Melt Spun Fibers

To measure the longitudinal image of the melt spun fibers, a digital microscope VHX-950 from Keyence Corporation was used. Fiber images were taken using different lenses and magnifications.

4. RESULTS AND DISCUSSION

4.1. Results of Melt Flow Characterization

The melt flow index value for neat compounds is given in Figure **2** and that for blend compounds is Figure **3**. The melt flow rate for neat TPS cannot be measured under the same parameters due to its very high viscosity. As we see from results in Figure **2**, the melt flow property of modified TPS was surprisingly improved with a MFR value of 232 g/10min as compared to neat TPS and neat PLA.

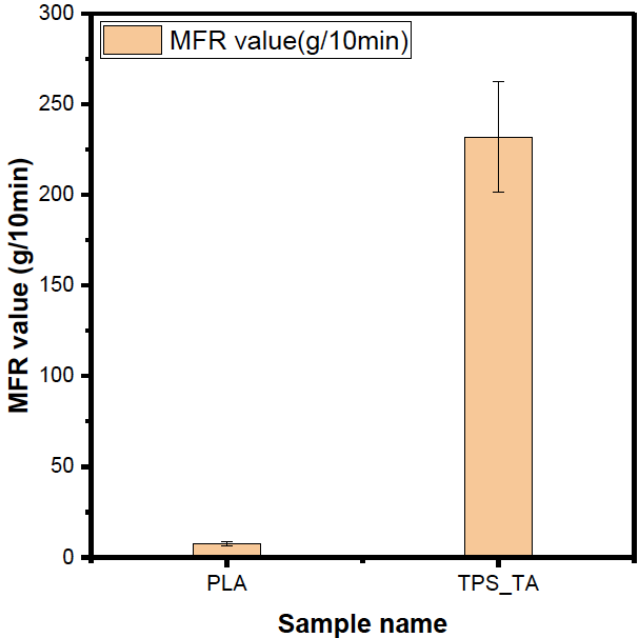

Figure 2: Melt flow rate results for TPS_TA and neat PLA.

This high melt flow ofTPS_TA is achieved due to a significant reduction in viscosity, which in turn is due to a reduction in molecular weight. The reduced molecular weight confirms the breakage of strong glycosidic bonds present in native starch by acid hydrolysis in the presence of tartaric acid. These confirm that carboxyl acids can promote the acid hydrolysis of starch molecular chains, causing the glycosides bond rupture and cleavage linkages [35]. The decrease in molecular weight of the polymer reduces the chain entanglement and results in exhibiting low shear viscosity and high flow properties. Figure **3** shows the MFR values for blend polymers prepared with and without TA addition. For the MFR analysis, a mixing ratio of 50/50 is used instead of the mixing ratio of 40/60. As we see from Figure **4**, the blend compounds prepared from TPS_TA have higher MFR values as compared to those prepared from neat TPS. The improved melt flow rate of blends prepared from TPS_TA, shows the effect of tartaric acid in facilitating better flow characteristics of blends overall. ANOVA analysis of MFR values shows significant differences between TA modified and unmodified samples for all blend ratios with a p value less than 0.05 at 95% confidence level. This confirms that tartaric acid significantly increasing the melt flow rate via a high reduction in starch viscosity.

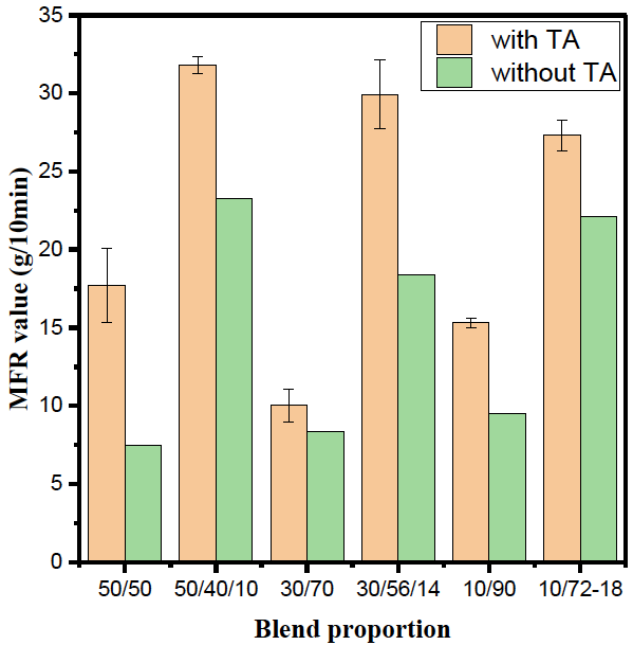

Figure 3: Melt flow rate for blend compounds.

4.2. Effect of Maleic Anhydride Grafting on Rheology of PLA

The effect of grafting on PLA rheology was studied using a dynamic oscillatory frequency sweep test done at a fixed strain of 1 % and a flow sweep test with steady shear rate varying from 0.1 – 100 /s. The rheology characteristics of neat PLA, grafted PLA (PLA-g-MA) and extruded PLA (as control) where extrusion is done using similar process conditions used for PLA grafting, were compared to see the effectiveness of grafting.

Figure **4** shows the rheological characteristics, shear viscosity, complex viscosity and storage modulus of neat PLA, grafted PLA and extruded PLA measured

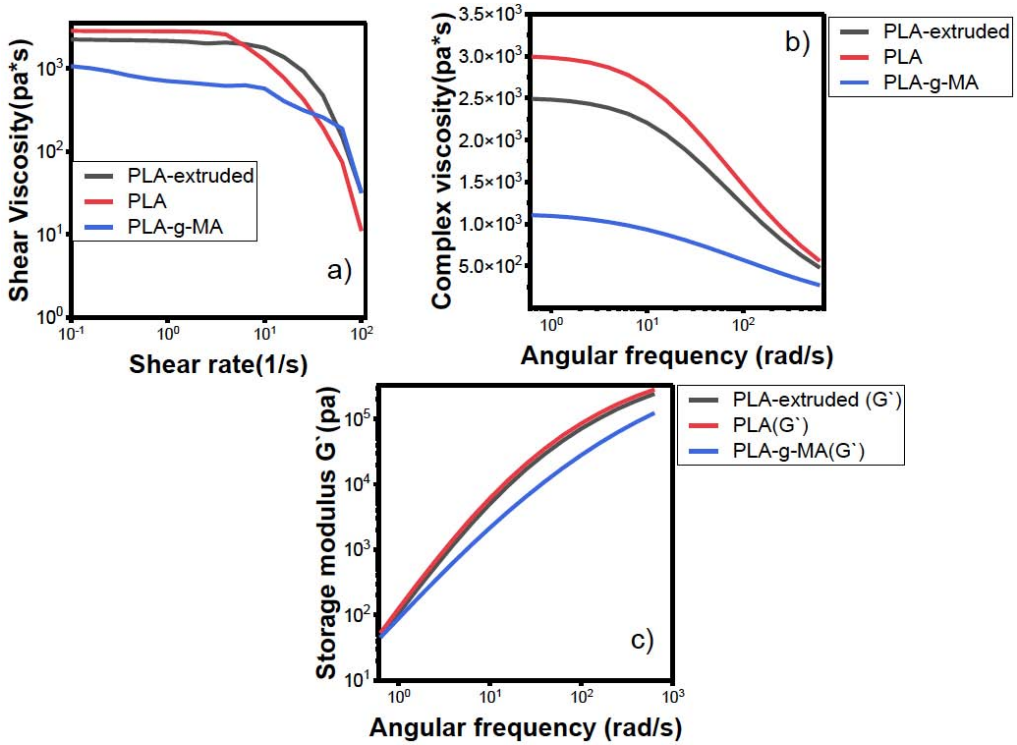

Figure 4: Rheology characteristics of neat PLA, PLA-g-MA and extruded PLA measured at 170 °C.

at 170 °C. As we see from Figure **4a**, **b**, the shear viscosity as well as complex viscosity of PLA-g-MA is much lower than that of neat PLA and extruded PLA which is most likely due to molecular weight reduction associated with grafting side effect. This result is in accordance with many previous research works [24, 25].

The reduced molecular weight of grafted PLA might be caused during grafting, where the anhydride groups of maleic anhydride facilitates the hydrolysis of PLA through chain scission [26, 27]. Figure **4c** also shows that the storage modulus of PLA-g-MA is lower than that of neat PLA as well as extruded PLA, confirming the lower molecular weight of PLA-g-MA, meaning less energy is required to break or loosen the comparatively less entangled chains.

4.3. Results of Shear Viscosity Measurement for TPS_TA and Blend Polymers

Rheology measurement of neat TPS was not possible due to very high viscosity, hence only TPS_TA and the blend compounds are used for rheology analysis.

Figure **5** shows the shear viscosity as a function of shear rate for different compounds measured at various temperatures. As we can see from Figure **5a**, **b** the shear viscosities of compounds decreased as the shear rate and temperature increased. The TPS_TA compound shows shear thinning or pseudoplastic flow which is characteristic of non-Newtonian fluids [40], where the shear viscosity decreases with increasing shear rate. It exhibited high sensitivity to shear stress, as can be seen by a sharp drop of viscosity with only a small variation in shear rate. The TPS_TA does not exhibit any viscoelastic plateau in the investigated shear rate range and is highly shear thinning. This is typical of branched or highly entangled polymer melts [41] confirming the highly entangled network structures of amylopectin and amylose along with lipids within the structure of starch. At higher temperature the shear viscosity is getting lower, maybe due to more starch crystallites melting at higher temperatures and increased molecular chain mobility as a result of temperature in addition to thermal degradation which may reduce molecular weight. In addition, an increase in temperature leads to decreased molecular cohesion or intermolecular interactions. TPS can be considered as a homogeneous system composed of a hard elastic network and soft amorphous regions. Amylose complex crystallites, highly entangled starch molecules, poorly plasticized starch-rich sites, or a combination of them could compose the hard elastic network. Soft amorphous regions could be composed of well-plasticized glycerol-rich starch [42].

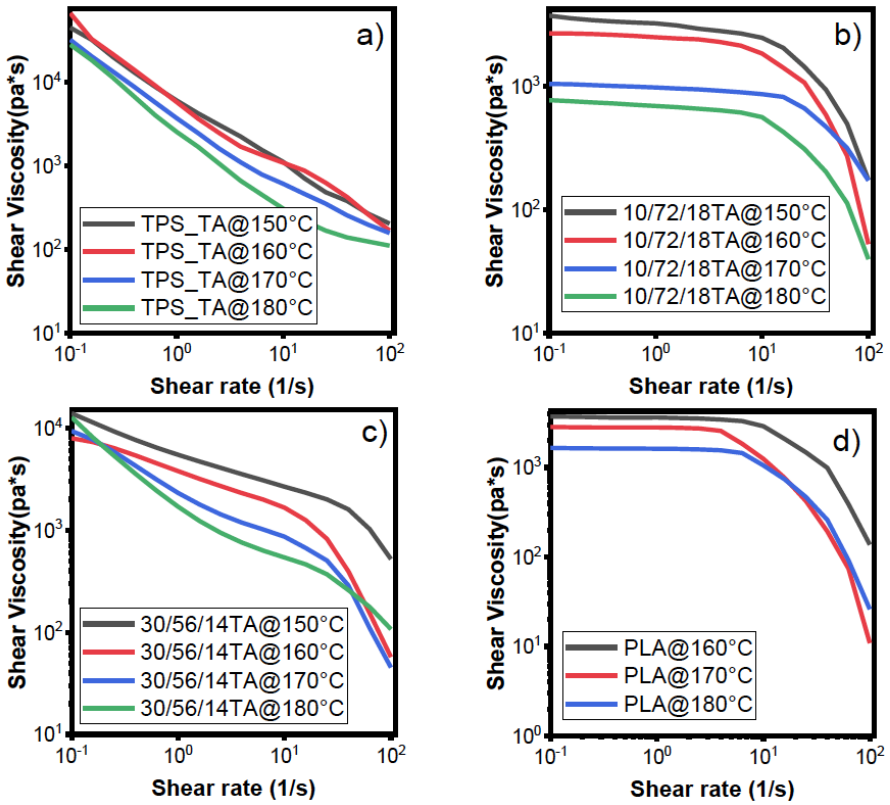

Figure 5: Effect of temperature on the shear viscosity of polymer compounds.

The shear viscosity of TPS_TA is much higher as compared to neat PLA and blend compounds (Figure **5a**). According to Gonzalez *et al*. [42], TPS does not follow the Cox-Merz relation. Under dynamic oscillatory conditions, the viscosity measured at low frequencies may not accurately represent the viscosity observed during steady shear flow at higher shear rates, leading to discrepancies with the Cox-Merz rule. Instead the Carreau model would be appropriate for TPS and TPS/PLA blend viscosity behavior modelling [43].

The Carreau model can be described using the following equation:

$$\eta = \frac{\eta^{\circ}}{\left[1+\lambda(\gamma)2\right]^{\frac{1-n}{2}}} \quad (2)$$

Where: η shear viscosity, η° zero shear viscosity, λ relaxation time, γ shear rate, n rate index

Table **4** shows the fitting parameters and values of the Carreau model for modified TPS and blend compounds analyzed.

As we see from Table **4**, the rate index (n) also referred to as power law index shows the smallest value (0.46) in the case of neat PLA which indicates that this compound has strong shear thinning behavior and is easier to process. Additionally, there is also a strong correlation (0.999) observed between the parameters confirming easy flow behavior and lower viscosity of this compound. As TPS_TA content increases, the rate index value increased gradually, confirming strong resistance to flow which might be due to more structured or networked molecular arrangement, possibly due to a higher TPS_TA content [44].

As we see from Figure **5b**, **d** shear viscosity of neat PLA and 10/72/18TA which stands for the blend 10TPS_TA/72PLA/18PLA-g-MA as defined in Table **3** follows a different behavior, i.e., characteristic Newtonian behavior with a viscoelastic plateau at a lower frequency. The shear viscosity does not drop immediately with increasing shear rate until it reaches a transition phase where the viscosity starts to drop with shear rate which is observed at all temperatures and may be caused by disentanglement of polymer chains during flow.

The shear viscosity as a function of the shear rate was comparatively studied for blend compounds with different TPS_TA proportions. Figure **6** shows the comparison of shear viscosity for different blend proportions of TPS_TA in the blend compounds and a

Table 4: Fitting Parameters for Carreau Model for Melt Spinnable Blend Compounds, Shear Viscosity which is Shown in Figure 6

Sample name	Temperature °C	Zero shear viscosity $\eta_{\circ}$ (Pa*s)	Relaxation time λ(s)	Rate index n	Correlation coefficient R^2
10/72/18TA	170	993	0.0583	0.529	0.995
30/56/14TA	170	44835	450	0.562	0.989
40/48/12TA	170	68615	531	0.548	0.999
PLA	170	2139	0.0369	0.46	0.999

The Cox-Merz rule states that the shear-rate dependence of the steady-state viscosity equals the frequency dependence of the complex viscosity (Cox and Merz,1958), 28, 619-622. http://dx.doi.org/10.1002/pol.1958.1202811812).

Carreau model fitted curve for the corresponding viscosity curves. As we see from the figure, the viscosity increases as TPS_TA content in the blend increases.

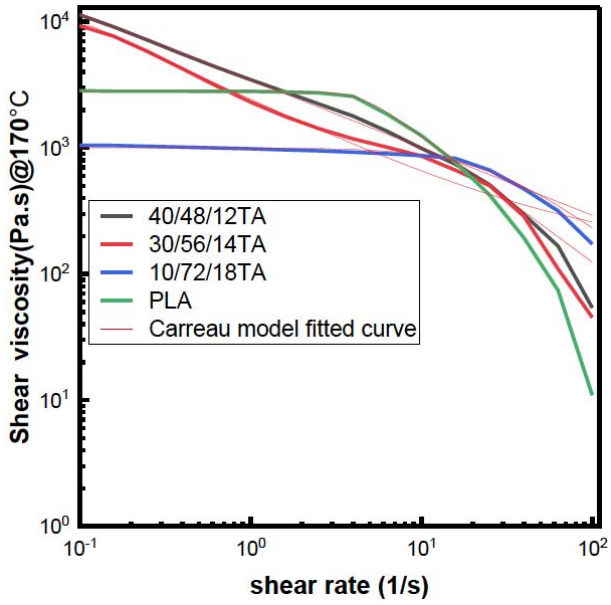

Figure 6: Shear viscosity curve showing the effect of blend proportion on shear viscosity at 170 °C and the corresponding Carreau model fitted curve.

The compounds 30/56/14TA and 40/48/12TA which represent 30TPS_TA/56PLA/12PLA-gMA and 40TPS_TA/48PLA/12PLA-g-MA respectively, has higher viscosity as compared to neat PLA and 10/72/18TA. These compounds exhibited non-Newtonian shear thinning behavior with a sharp drop in viscosity at higher shear rates. The compounds with higher TPS content are highly sensitive to shear rate applied, as the viscosity starts to drop with a small shear force applied. The shear viscosity of 10/72/18TA is lower than that of neat PLA, also the shear thinning started later. This might be due to a reduction in molecular weight of 10/72/18TA and or polymer chain degradation during blending or plasticizer migration causing easy chain mobility in PLA. Polymers with higher molecular weight or broader molecular weight distribution generally exhibit shear thinning at lower shear rates [45] and this may also be a reason for the low tensile strength of melt spun fibers from this compound even though higher take-up speed was achieved.

Figure **7a-d** shows the effect of TA and PLA-g-MA on the shear viscosity of blends. As we see from Figure **8a**, **b**, the compatibilized and non- compatibilized blends with 40%, 30% and 10% TPS_TA content have different viscosity values. The viscosity of compatibilized blends 10/72/18TA, 30/56/14TA and 40/48/12TA is lower than that of non-compatibilized blends 10TPS_TA/90PLA, 30TPS_TA/70PLA and 40TPS_TA/60PLA respectively which are defined in Table **3**, confirming that PLA-g-MA is distinctly influencing viscosity of the blends. The low viscosity of compatibilized blends is associated with better miscibility between TPS_TA and PLA. The better miscibility can be achieved by small microstructure formation leading to homogeneous distribution of blend components. This in turn may lead to a dominant PLA phase in the blend which then leads to dominance of the low viscosity of PLA as compared to TPS_TA.

In Figure **7c**, **d** the shear viscosity of blends with and without TA are compared. The addition of TA in TPS lowered the shear viscosity of blends but its effect is very minimal in case of uncompatibilized blend compounds (Figure **7c**) as compared to the compatibilized blends (Figure **7d**). This confirms the influence of compatibilization on the reduction of shear viscosity. The addition of TA improved the melt flow character of TPS more significantly as was observed in the MFR results. However, the influence of TA in case of blends is not significant, as only a slight reduction in viscosity was observed. This might be due to physical network formation between the blends which may reduce flow characteristics as compared to TPS_TA, in addition to the high possibility of plasticizer migration in

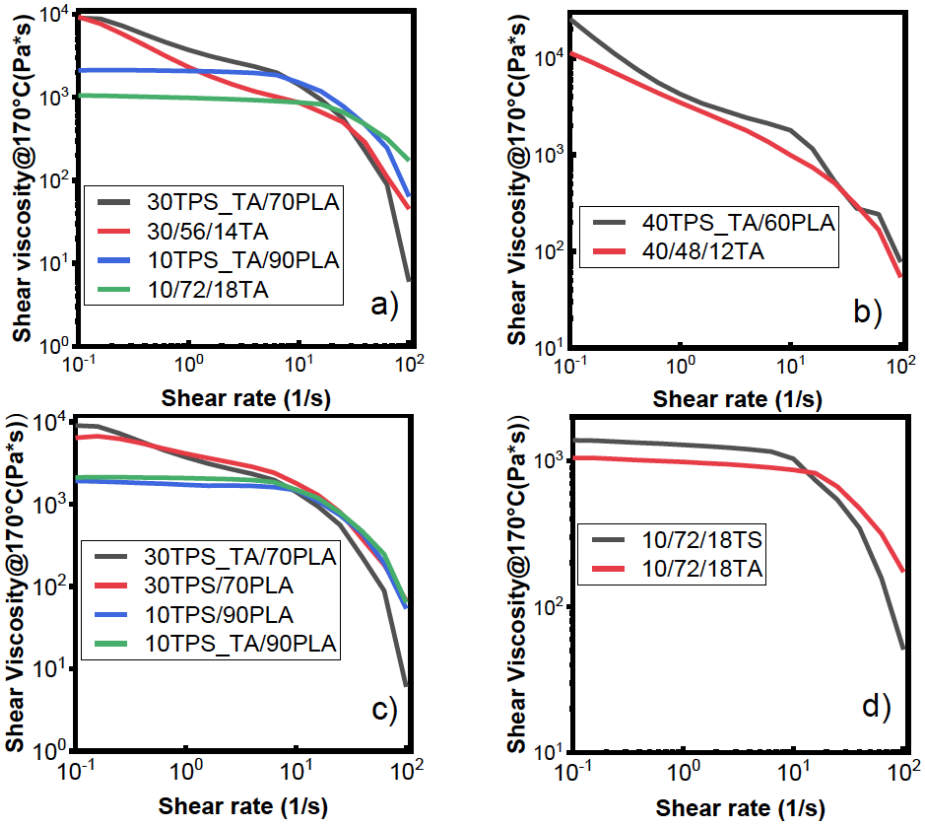

Figure 7: Effect of TA and PLA-g-MA on shear viscosity of blend polymers.

case of blends as compared to the acid modified TPS_TA [46]. It may be derived from Figure **7d**, that the significant reduction in shear viscosity of10/72/18TA when compared to 10/72/18TS is associated to with a coupling effect of TA in the blend [23, 31] confirming that TA also acts as a coupling agent aside from reducing the high viscosity of native starch.

4.4. Results of Complex Viscosity (η*)

Figure **8a**, **b** shows the complex viscosity (η*) as function a of angular frequency (ω) for TPS_TA and 10/72/18TA compounds at various temperatures. As we see from the complex viscosity curve, the viscosity decreases as temperature and angular frequency increase which is characteristic of non-Newtonian shear thinning behavior. Regarding the effect of TA modification, Figure **8d** shows the complex viscosity of TA modified and unmodified blends. As we see from the figure, the TA modified and unmodified blends 10TPS_TA/90PLA and 10TPS/90PLA show overlapped curves which indicates that there is no significant variation in the complex viscosity of these blends. However, the 30TPS_TA/70PLA and 30TPS/70PLA blends show that the TA modified one has a higher complex viscosity than the unmodified one, indicating a nucleating effect of TA promoting network structure between the blend components.

In case of the blends, Figure **8c** shows that neat PLA and 10/72/18TA exhibited characteristics of Newtonian behavior with a viscosity plateau at lower frequency, while 30/56/14TA and 40/48/12TA exhibited non-Newtonian shear thinning behavior in the entire frequency range. The complex viscosity of 10/72/18TA when compared to neat PLA and other blends is the lowest. The low viscosity of 10/72/18TA as compared to neat PLA may be due to migration of plasticizer from a TPS_TA dispersed phase into the PLA matrix, lubricating PLA chains, increasing chain mobility and reducing the complex viscosity [48].

Additionally, Figure **8d** shows that compatibilized blends 10/72/18TA and 30/56/14TA have lower complex viscosity as compared to the non-compatibilized blends 10TPS_TA/90PLA and 30TPS_TA/70PLA. This indicates that compatibilization with PLA-g-MA is distinctly influencing the viscosity of the blend polymers. The reduced viscosity may be related to a better miscibility of TPS_TA and PLA, resulting in a small microstructure phase in which PLA dominates the rheological properties.

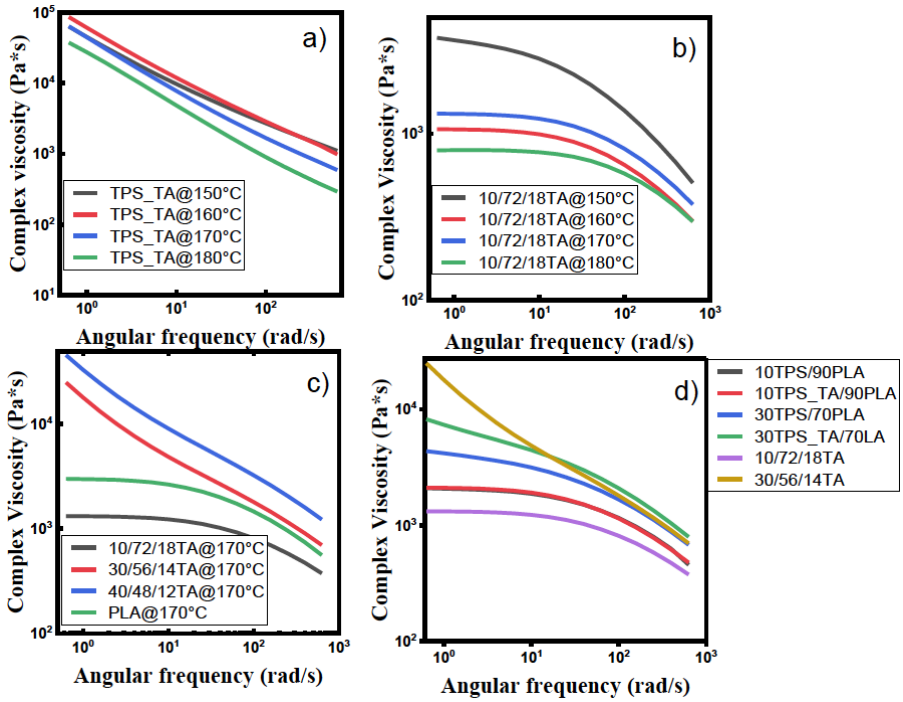

Figure 8: Effect of temperature, blend proportion, TA addition and compatibilization on complex viscosity.

4.5. Results of Storage Modulus and Loss Modulus (G` and G``) Measurements

The viscoelastic characteristics of TPS_TA, neat PLA and TPS_TA/PLA blends are studied. Figure **9** shows the storage modulus (G`) and loss modulus (G``) of TPS_TA at various temperatures. According to previous research works, TPS has been found to display a gel-like viscoelastic behavior [42]. Such rheological behavior has been related to the formation of a crystalline elastic network produced by the complexation of amylose molecules with lipid and physical entanglement of starch chains caused by its very high molecular weight. As we can see from the curve, the storage modulus (G`) (also called elastic modulus) and loss modulus (G``) (also called viscous modulus) have higher values at 170 °C. At this temperature the storage modulus is at a higher value than the loss modulus indicating that the material is in a solid like (elastic) state within the entire frequency range with no crossover point.

Additionally, from Figure **9**, at 160 °C the storage modulus dominates at lower shear rates indicating that the material is in a solid like state at lower shear rates. As the shear rate increases, there comes a crossover point which is the transition point for materials from a solid like state to viscous/liquid like state where the loss and storage modulus have equal values. After the crossover point the loss modulus dominates, indicating that the material is at a liquid like or viscous state at higher shear rates. This results because the stored elastic stress relaxes through the rearrangement of the microstructure and transforms into viscous stress. This might indicate a favorable range of temperature and shear for processing this compound.

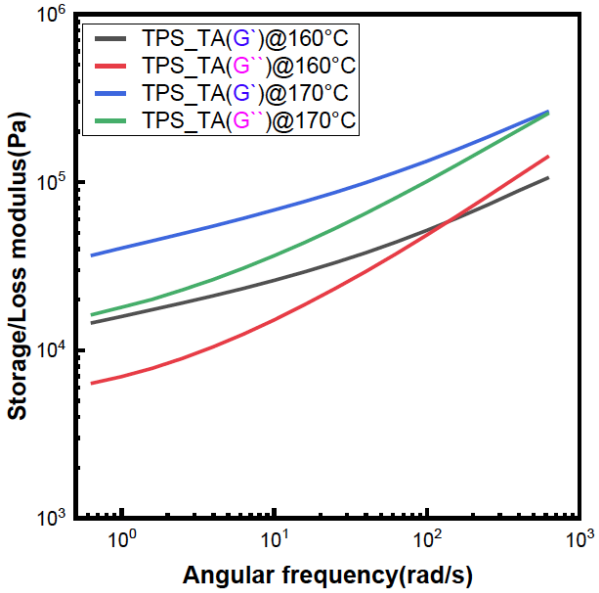

Figure 9: Comparison of storage/loss modulus of TPS_TA at different temperatures.

Figure **10** shows the comparison of storage/loss modulus as a function of angular frequency for TPS_TA and PLA at 170 °C. As we see from the figure,

the slope of the PLA storage modulus (G') is relatively steep at lower frequencies and flattens out at higher frequencies. This indicates that PLA is relatively rigid and has a strong elastic response at low frequencies. As the angular frequency increases, the material still shows elasticity but to a lower degree. Further comparison of the curve slopes shows that the storage modulus (G') of TPS_TA has a less steep slope compared to that of neat PLA, indicating reduced stiffness. A comparison of loss modulus curves shows that the loss modulus (G'') for PLA exhibits a relatively moderate increase with increasing frequency, indicating that PLA has some viscous behavior, but which is not as dominant as its elastic behavior. The loss modulus (G'') for TPS_TA increases more steeply with increasing frequency as compared to neat PLA, suggesting that TPS_TA has a higher energy dissipation (viscous behavior).

Further, for neat PLA the loss modulus (G``) is higher over the entire range of angular frequency, indicating that neat PLA is at a viscous or liquid like state throughout the entire range with a crossover point at the end of applied angular frequency which indicates the material becomes elastic as we further increase the angular frequency. However, in case of TPS_TA, the storage modulus (G`) dominates over the loss modulus (G``) over the entire range of angular frequency indicating that TPS_TA remains solid like or elastic at this particular temperature throughout the entire range of angular frequency studied.

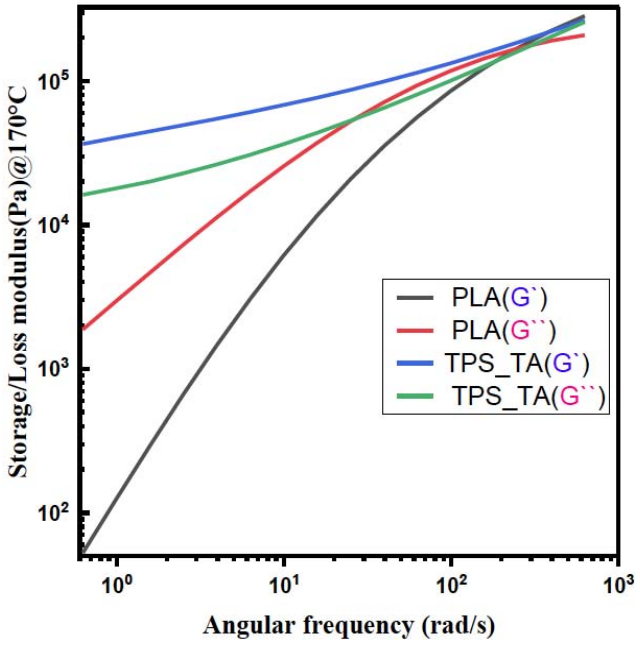

Figure 10: Comparison of storage modulus and loss modulus of TPS_TA and PLA at 170 °C.

Figure **11** shows the effect of blend proportions on storage modulus (G`) and loss modulus (G``) of blend polymers. As we see from the figure, generally the modulus value increased proportionally to the angular frequency. This behavior is typical in thermoplastics, because energy input is required to increase the mobility of polymeric chains [17].

Further, the storage and loss modulus values increased as TPS_TA content increased in the blend. At higher TPS_TA contents, two crossover points were observed within the given frequency range for 30/56/14TA and 40/48/12TA. However, in the case of 10/72/18TA (G``) is dominating throughout the entire frequency range indicating that the material is at a viscous state. With 30/56/14TA and 40/48/12TA, the (G`) dominates at lower frequency and a crossover point where G`= G`` comes at frequency of about 10 rad/s, indicating a transition phase from elastic to viscous behavior and this viscous phase dominated for some range of frequency and turns again to elastic behavior after the second crossover point that occurs at about 160 rad/s indicating dominance of an elastic phase at higher frequencies. At frequencies below the first crossover point, the polymer can have a strong network of starch associated with higher TPS_TA content in the blend and there is no possibility of chain relaxation. However, as the frequency increases, the polymer chains get the possibility to relax and start to exhibit viscous characteristics.

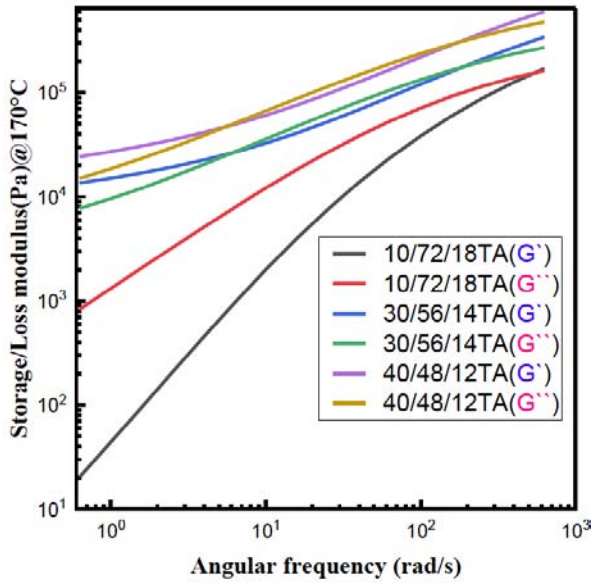

Figure 11: Comparisons of storage/loss modulus for different blend proportions.

The occurrence of two crossover points (G' = G'') at different frequencies within the studied range may

indicate the change in molecular weight, while the crossover point change at different moduli indicates a variation in molecular weight distribution [49]. The lower the frequency of crossover, the higher the molecular mass [50]. On the other hand, two factors affect the G`: (1) the number of oriented chain segments will increase as the shear rate increases and, (2) simultaneously, the oriented chain segments will have less time for disorientation. Therefore, at high frequencies, entangled chains have a short time to relax and increase the amount of storage modulus [51]. At frequencies higher than the crossover point, the material is unable to relax sufficiently quicky within the timescale of the applied oscillations and exhibits significant elastic behavior (G' dominates over G"). Conversely, at lower frequencies, the relaxation behavior is faster than the applied oscillations and the material exhibits viscous characteristics [40].

The effect of TA and the PLA-g-MA compatibilizer on blends is given in Figure **12**.

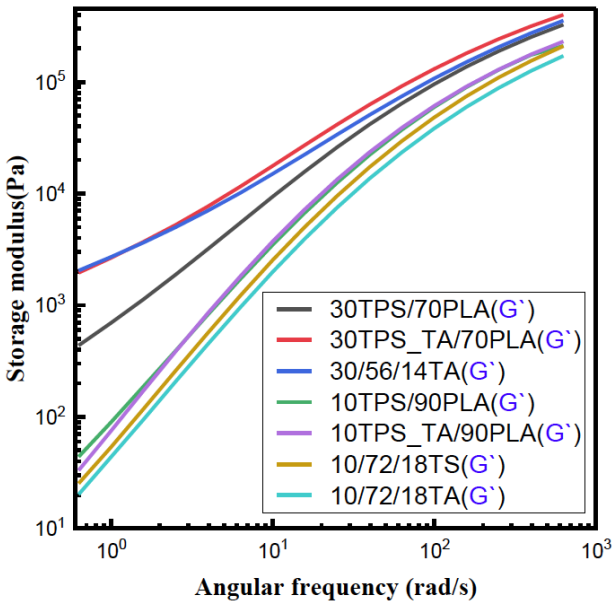

Figure 12: Effect of TA addition and compatibilization on storage modulus.

The addition of compatibilizer PLA-g-MA in the blends resulted in a reduced (G`) as can be seen for 30/56/14TA and 10/72/18TA compared to the non-compatibilized blends of the same blend proportion. This is because the PLA-g-MA compatibilizer promotes the bridging and entanglement of TPS and PLA chains in the blend [52]. Consequently, it helped with recovery of the deformation during shearing and hence reduced the storage modulus. Moreover, since the shearing deformation of TPS chains was easier to recover, it would inherently dissipate less energy and reduces the G``. Comparison of blends prepared from unmodified or neat TPS and TPS modified with TA shows that the neat blends have a slightly lower G` as seen in the case of 30TPS/70PLA and no change in storage modulus in the case of 10TPS/90PLA. The slightly lowered G` may be related to TA acting as a coupling agent improving miscibility between TPS and PLA, raising the role of TPS in the blend and causing higher G` in the blends because of better TPS_TA dispersion within the blends. In other words, in case of the unmodified TPS, i.e., neat TPS/PLA blends, the PLA phase is dominating due to relatively poor miscibility between the blend partners and hence exhibiting a lower G` as compared to the blends with TPS_TA.

4.6. Results of Structural Characterization

Fourier transform infrared spectroscopy (FTIR) is utilized to characterize the variations in functional groups of native starch during thermoplasticization (TPS), TA modification (TPS-TA) and during melt blending with PLA. Figure **13** shows the FTIR spectra for native starch, TPS, TPS_TA and neat PLA. As we see from Figure **13a** native starch has a characteristic broad peak at 3281 cm^{-1} related to O-H stretching, this peak shifted to a higher value of 3287 cm^{-1} in case of TPS, indicating weakening of the strong hydrogen bonds and/or glycosidic bonds between starch chains as a lower wave number indicates stronger interaction [37, 38] due to starch granular destruction during extrusion in the presence of a plasticizer. During the processing, granular starch is de-structured and plasticized, but it is also partially depolymerized and transformed into a semi-crystalline structures in a molecular network stabilized by hydrogen bonding between itself and the plasticizers [54].

Another new high intensity peak in TPS, found at 1016 cm^{-1} corresponds to the newly formed hydrogen bonds between the plasticizer glycerol and the C−O group of native starch or deformation of C−O glucose rings. Similar results have been observed by previous research works [52, 53]. The O-H peak was further shifted to a higher wave number of 3300 cm^{-1} in the case of TPS_TA confirming further destruction or weakening of more hydrogen bonds due to acid hydrolysis action of tartaric acid which is confirmed by rheology measurements with high melt flow and reduced viscosity. Thermoplastic starch is in a gelatinization state with significant volume expansion and results in improving the acid hydrolysis degree by [H+]. Thus, starch glycosides bond rupture happens

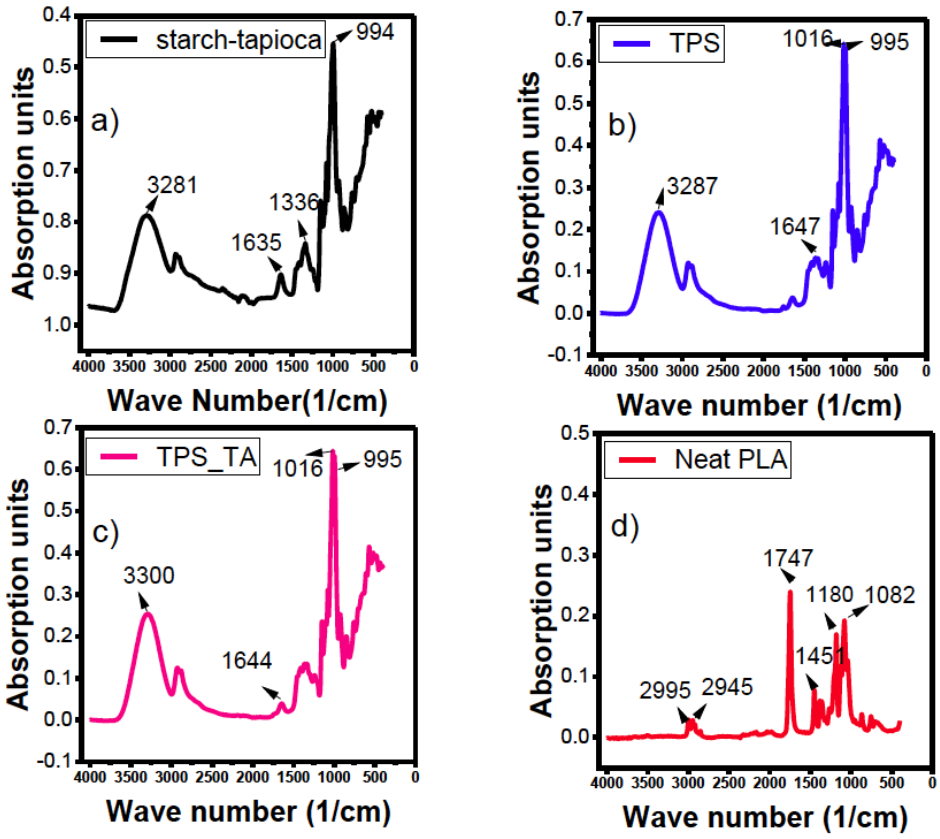

Figure 13: FTIR spectra for native starch, neat TPS, TPS_TA and neat PLA.

within chains leading to glycosidic linkage cleavage and hence reduced molecular weight. Additionally glycosidic linkage rupture may for more free -OH groups that leads to higher -OH stretching peak wave number. However, the expected C=O functional groups from acid hydrolysis at a wave number range of 1735 – 1745 cm^{-1} are not observed in the analysis which may be due the low TA content of 0.5%w/w in the TPS_TA. According to Zhang *et al*. [47], who analyzed different contents of TA in TPS, the acid functional groups were not detected by FTIR analysis with low TA content, even though there was a significant reduction in molecular weight of the analyzed compound.

The FTIR spectra of neat PLA revealed a characteristic absorption peak at 1747 cm^{-1} which was not found in native starch, TPS or TPS_TA. This peak is associated with carbonyl C=O stretching, whereas the bands at 1180, 1082, and 1043 cm^{-1} correspond to the C−O−C stretching vibration of PLA ester groups [57].

Figure **14** shows the comparison of FTIR spectra for compounds with different TPS_TA content which are used in melt spinning. As we can see from the figure, most of the blend compounds exhibited the presence of O-H stretching functional groups associated with TPS, and carbonyl stretching functional groups at a peak of about 1747 cm^{-1} associated with the PLA phase. However, the blend compound 10/72/18TA does not exhibit the O-H stretching functional groups clearly, which may be due to fine distribution of TPS_TA within the blend as it is a minor component. In addition, in the case of blends, the O-H functional group shows

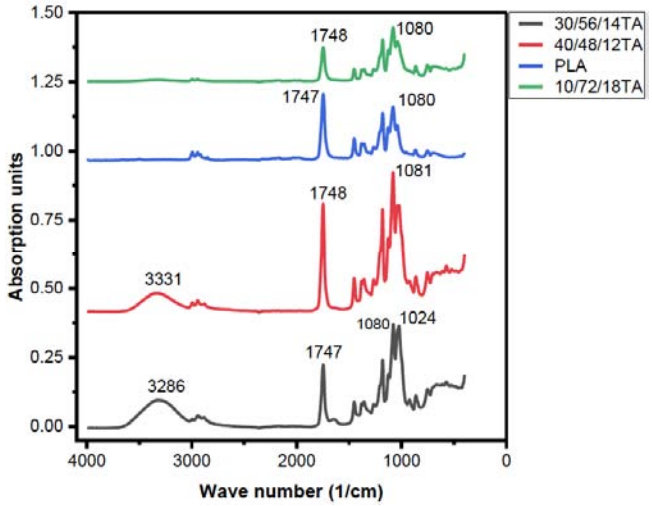

Figure 14: Comparison of the effect of blend proportion on FTIR spectra.

different peak intensities based on TPS_TA content. The peak intensity increased as TPS_TA content increased. At a lower TPS_TA content, the peaks are very similar to that of neat PLA. Neat PLA does not exhibit a O-H peak while it shows small intensity peaks at about 2994 cm^{-1} and 2944 cm^{-1} associated with C-H stretching and a high intensity peak at 1747 cm^{-1} associated with the carbonyl functional groups C=O stretching.

Figure **15** shows the effect of TA and compatibilizer on the FTIR spectra of blend polymers. In Figure **15a**, **c**, the spectra of 10TPS/90PLA and 30TPS/70PLA with and without TA modification is compared. Generally, we can see that the O-H peak intensity in 30TPS/70PLA blends is higher as compared to10TPS/90PLA blends regardless of TA modification or compatibilization. From the figure it is also clear that the intensity of the O-H peak in TA modified blends is higher than the one in those without modification which show better interaction of TPS_TA with PLA in the blends forming additional O-H groups. This might be due to a coupling effect of TA which is in agreement with rheology results.

In Figure **15b**, **d** the spectra of compatibilized blends 10/72/18TS and 10/72/18TA, 30/56/14TS and 30/56/14TA are compared. As can be derived from the spectra, the compatibilized blend with TA modification (10/72/18TA) shows a very low intensity O-H peak as compared to the unmodified blend 10/72/18TS indicating much better miscibility between TPS_TA and PLA, hence the FTIR spectra shown is similar to that of neat PLA with a PLA phase dominance in the blend. This also confirms the coupling effect of TA aside from the compatibilizing effect of PLA-g-MA present in both cases. 30/56/14TA shows a slightly lower O-H peak intensity as compared to 30/56/14TS which again shows a relatively better miscibility between TPS_TA and PLA, revealing the dominance of the PLA phase.

4.7. Results of Melt Spinning Trials

Melt spinning trials on the piston type monofilament spinning device were done with the following polymer compounds: 10/72/18TA, 30/56/14TA, 40/48/12TA and neat PLA. The selection was based on spinnability trials performed on non-standard filament makers' devices, which found that the compatibilized blends were better spinnable. Table **5** shows the parameters used for melt spinning along with maximum take-up speed achieved, and diameter of the melt spun fibers at different take-up speeds. As we see from the table, maximum take-up speeds of 300 m/min, 700 m/min and 2000 m/min were achieved for blends with 40%w/w, 30%w/w and 10%w/w TPS_TA content,

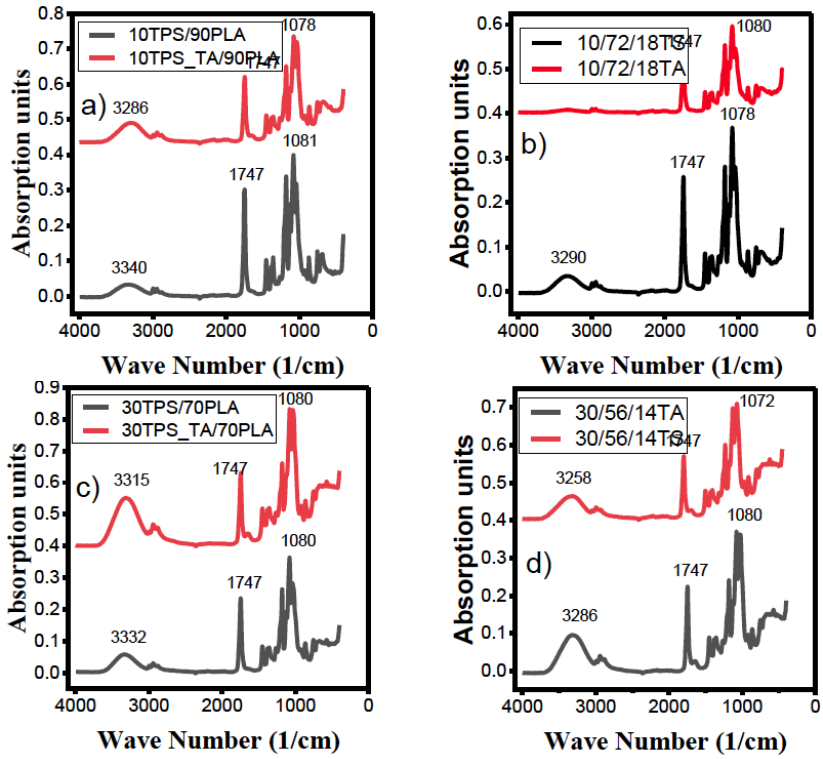

Figure 15: Comparison of FTIR spectra for compatibilized/uncompatibilized and TA modified/unmodified blends.

Table 5: Diameter of Melt Spun Fibers along with Process Parameters and Maximum Take-Up Speed Achieved

Blend proportion	Designation	Through put rate (cm^3/min)	Temperature used (°C)	Maximum take up speed (V) achieved (m/min)	Fiber diameter (μm) at different V
40TPS_TA/48PLA/12 PLA-g-MA	40/48/12TA	0.785	180	300	V300=46 V100 =92
30TPS_TA/56PLA/14 PLA-g-MA	30/56/14TA	0.785	180	700	V700=13 V100=85
10TPS_TA/72PLA/18 PLA-g-MA	10/72/18TA	0.785	180	2000	v200=12 V100=84
PLALX530	PLA	0.785	180	2000+	V200=12 V100=83

respectively. The diameter of the melt spun fibers was found vary based on take-up speed at constant temperature and throughput rate, with diameters increasing as take up-speed decreases. The diameters of fibers melt spun from blends with higher TPS_TA concentration was found to be coarser regardless of take-up speed used.

Figure **16** shows images from melt spun fibers produced via the piston type monofilament fiber melt spinning device. As we see in Figure **16a**, melt spun fibers from 40-48-12TA, containing 40%w/w TPS_TA, show good appearance with a coarser surface resembling commercial cellulosic fibers. This opens the possibility of melt spinning fibers from TPS/PLA blends with even higher TPS content. Pressure during melt spinning was found to be good with values in between 40–50 bar compared to literature values However, during filament melt spinning, heavy smoke was observed as a result of the plasticizer glycerol evaporating which was observed by other researchers as well during TPS based film extrusion [58]. The higher TPS content in this blend may have resulted in more glycerol vapor formation during melt spinning. Furthermore, the polymer melt emerges inhomogeneously and the filament diameter was observed to vary which may be due to the high content of starch in this blend resulting in a different morphology in the blend and affecting polymer melt flow behavior. The melt spun fibers from 30/56/14TA containing 30%w/w TPS_TA show a similar appearance to commercial synthetic fibers with a finer surface diameter. The pressure during melt spinning was better with a value of 30 bar and the melt emerged homogeneously at low winding speed but as the speed increases, inhomogeneity developed. There was clear smoke developed in this case as well, however the smoke was less as compared to the blend with 40% TPS_TA. The fibers with 10%w/w TPS_TA were closely similar in appearance to those of neat PLA but whiter in color since the neat PLA fibers were observed to be colorless and transparent. The pressure was normal, and no smoke was observed during melt spinning, higher winding speed was also achieved showing more successful melt spinning of fibers from this compound which will diversify the application areas of the melt spun fibers.

4.8. Results of DSC Characterization of Melt Spun Fibers

Changes in the thermal properties (T_g and T_m) and the crystallinity of the polymer chains due to processing conditions were determined using a differential scanning calorimeter (DSC).

Figure **17a-d** shows the DSC second heating curves for melt spun fibers prepared using different take-up speeds. As we see in Figure **17a**, the DSC curve for 10/72/18TA shows a T_g of 60.4 °C, furthermore at lower take-up speed the fibers clearly exhibit two melting peaks at a temperature of 155 °C and 161 °C. This is attributed to two forms of crystal formation in the PLA phase. The crystallization peak occurred at a temperature of 112 °C and the polymer has a calculated percentage crystallinity of 1.74%. At higher take-up speed the glass transition and melting temperature increases and crystallization remains the same which is associated to greater crystal formation as a result of increased molecular orientation at higher take-up speed, this can increase the melting temperature, as more energy is needed to melt the crystals [59]. In the case of 40/48/12TA, at all take-up speeds, the polymer shows two clear melting peaks. The glass transition and melting peak values are similar at lower take-up speed. But at a higher take-up speed of 300 m/min, the crystallization peak was shifted to a lower value.

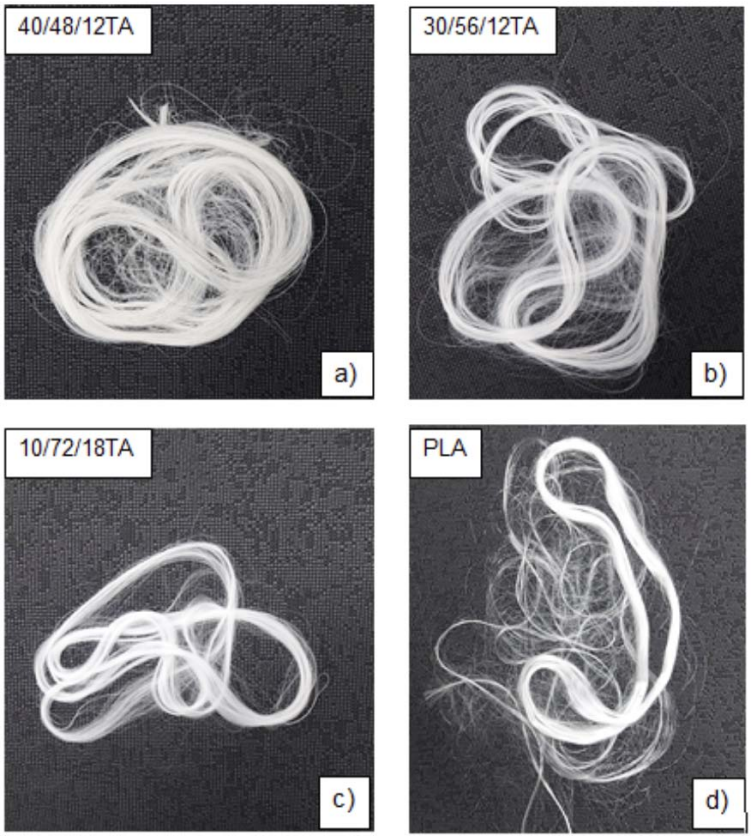

Figure 16: Images of melt spun fibers from different blend compounds and neat PLA.

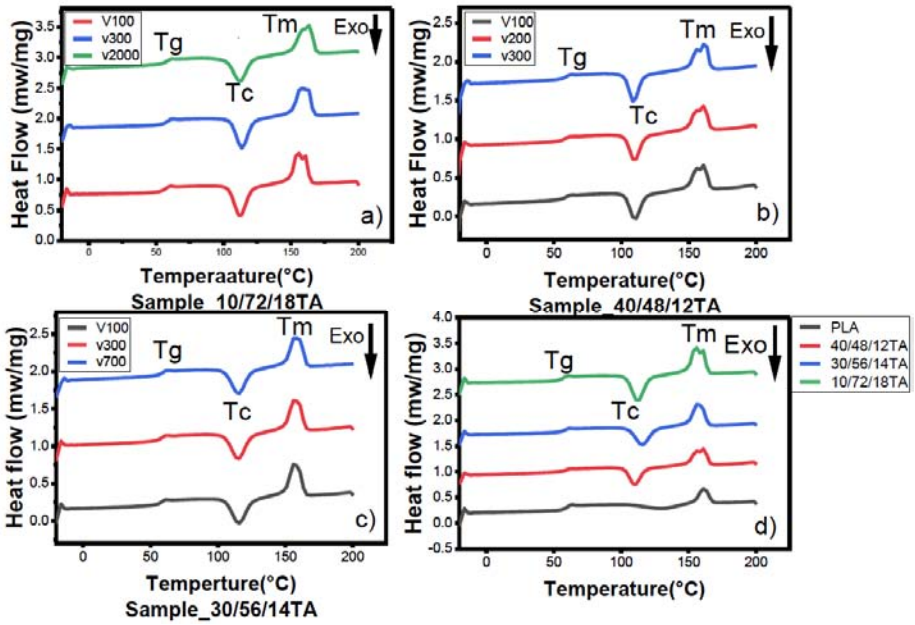

Figure 17: Effect of take-up speed and blend proportion on thermal transition.

With regard to blend proportion, as we see in Figure **17d**, the addition of TPS_TA resulted in the occurrence of a crystallization peak which was not observed on neat PLA this may be attributed to a nucleating effect of TSP or plasticizer migration from TPS to the PLA phase initiating molecular chain mobility and facilitating crystallization [60]. As blend proportions of TPS_TA change from 10%w/w to 40%w/w, the peak intensity changed slightly and there are double melting peaks in the case of 10% and 40% TPS_TA content which might

Table 6: DSC Results of Melt Spun Fibers

Compound name	T_g	T_{m1}	T_{m2}	T_{cc}	X_c%	ΔH_m	ΔH_c
Comparison of different blend proportions at take up speed of 100m/min							
10/72/18TA	60.4	155	161	112	1.75	34.83	33.7
30/56/14TA	62	157	-	115	1.55	27.11	26.32
40/48/12TA	63	161	156	110	0.73	22.39	20.978
PLA	63	161	-	-	-	-	-
Comparison of different take up speed v(m/min)							
10/72/18TAV100	60.4	155	161	112	1.74	34.83	33.7
10/72/18TAv200	61	157	162	113	3.52	34.98	32.03
10/72/18TAv300	62	157	161	113	3.7	35.39	32.27
10/72/18TAv2000	62	157	163	112	6.4	35.75	30.35
30/56/14TAv100	62	157	-	115	1.55	27.11	26.32
30/56/14TAv200	62	156	161	114	3.48	28.86	26.59
30/56/14TAv300	62	157	-	115	4.94	28.35	25.13
30/56/14TAv700	62	156	161	114	6.27	28.27	24.18
40/48/12TAv100	63	156	162	110	0.73	23.03	22.62
40/48/12TAV200	62	156	161	110	3.7	22.75	20.65
40/48/12TAv300	62	155	161	108	3.52	23.035	21.056

be associated wth orientation of polymer chains during melt spinning leading to formation of imperfect crystals that may melt at different temperatures [54, 55]. However, there is only a single melting peak in the case of 30%w/w TPS_TA content which may indicate reduced phase separation and better miscibility of this blend.

The DSC parameters for melt spun fibers are given in Table **6**. As we see from the values in Table **6**, the percentage crystallinity of melt spun fibers is less than 10% in all cases which may be caused by the amorphous nature of the PLA used in this study, in addition to the amorphous nature of TPS_TA. The addition of TPS_TA increased the crystallinity of PLA as compared to neat PLA. As we see from the table values, most of the compounds exhibited two melting peaks (T_m) regardless of blend proportion and take-up speed used, which might be attributed to the development of new forms of crystals that can melt at different temperatures which results from process induced crystallization during melt spinning [63].

As we see in the table, T_g shifted from 60.4 °C to about 62 °C as take upspeed increases from 100 m/min to 300 m/min in case of 10/72/18TA which may be attributed to increased molecular orientation as a result of higher take-up speed, though the change in T_g is small which we associated to less structural arrangement and molecular orientation during take. The increased molecular orientation makes polymer chains align in specific directions which may restrict polymer chain mobility; as a result T_g increases because more energy is required to achieve segmental motion [64]. In case of blends with higher TPS_TA content there is no shift in T_g value as take-up speed increases from 100 m/min to 300 m/min which might be attributed to a higher TPS_TA content forming network structures and limiting molecular chain mobility which in turn can raise the T_g value regardless of take-up speed. This shows that the adhesion between phases which results from interfacial interaction between phases is higher than the stretching force applied during take-up which is expected to give molecular mobility [55, 58]. In another case, the T_g increased from 60.4 °C to 63 °C for a given take-up speed as TPS_TA content increase from 10% to 40% which may be attributed to the formation of a more rigid amorphous TPS phase in case of higher TPS_TA content that may limit overall mobility of polymer chains resulting in higher T_g [66].

4.9. Results of Tensile Strength of Fibers

Table **8** shows the results of tensile strength measurement for some of the melt spun fibers. As we

Table 7: Tensile Properties of Melt Spun Fibers

Compound name	Take up speed (m/min)	Average tensile strength (cN/tex)	Average elongation at break (%)	Average fiber linear density (Tex)
Neat PLA	100	4.61	2.34	4.61
	200	5.63	2.93	4.17
10TPS_TA/72PLA/18PLA-g-MA	50	3.57	3.78	16.62
	100	3.48	3.64	8.50
	200	3.74	2.32	4.39
30TPS_TA/56PLA/14PLA-g-MA	50	2.87	2.01	15.10
	100	3.4	8.3	9.38
	200	2.36	10.8	9.39
40TPS_TA/48PLA/12PLA-g-MA	50	1.43	4.1	20.73
	100	-	4.1	14.1-
	200	1.83	4.2	11.80
	50	1.92	5.9	15.1

can see, the tensile strength and elongation at break vary as take-up speed varies and average linear density of fibers decreased as take up speed increases.

The tensile strength of fibers increased as take-up speed increases even though it does not follow a uniform trend due to non-uniformity of the melt spun fibers surface diameter. The increased tensile strength with increased take-up speed has also been observed by previous researchers [67]. The tensile strength of fibers is reduced as TPS_TA content increases, also linear density of the fibers increased as TPS_TA content increases.

Figure **18** shows a diagrammatic illustration of the tensile strength and elongation at break of melt spun fiber from different compounds using varying take-up speeds. As we see from the figure, the elongation at break incerases as TPS_TA content increases, however it does not follow a uniform trend due to non-uniformity on fiber surface. The tensile strength of melt spun fibers decreases as TPS_TA content increases in the blend. The variation on tensile strength as blend proportion changes was analyzed using ANOVA analysis which revealed that there is significant variation in tensile strength with a p value of 0.01 which is less than 0.05 at 95% confidence limit, confirming significance of the variation.

4.9. Results of Microscopic Images of Melt Spun Fibers

Longitudinal images of melt spun fibers from different samples are shown in Figure **19**. As we see from Figure **19a** the melt spun fibers from 10/72/18TA have a uniform and smooth surface with a nearly colorless appearance, while fiber from neat PLA (Figure **19d**) have a very smooth and uniform surface with a colorless appearance and a relatively finer surface diameter. The melt spun fibers from 40/48/12TA (Figure **19c**) have a coarser surface with white color and with a lot of bids or non-uniformities on the fiber surface. As also observed in the rheology results, the viscosity of this blend compound was higher which is contributing to the coarser surface of the fiber. When the viscosity of the polymer blend is increased, the resistance to flow during extrusion also increases which can lead to thicker fibers. Generally, as TPS_TA content increases, the fibers are getting a

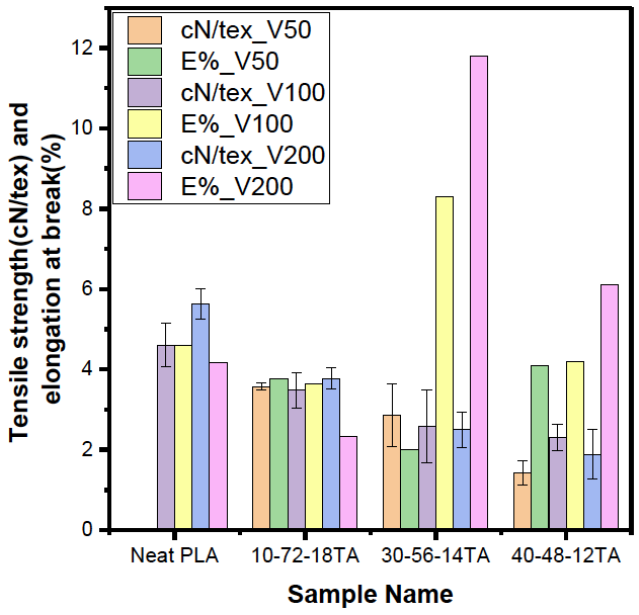

Figure 18: Comparison of tensile strength and elongation at break for different samples at various take-up speed.

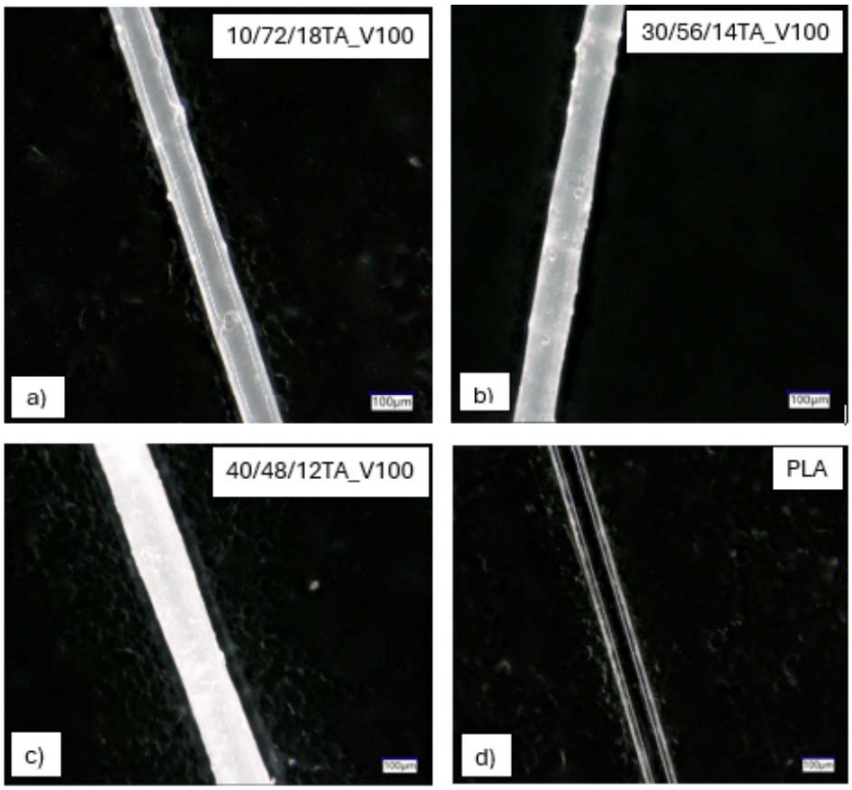

Figure 19: Optical microscope images of melt spun fibers.

coarser surface and whiter color with increased non-uniformity as seen in the microscopic images.

4. CONCLUSION

The study shows the possibility of further modifying thermoplastic starch to improve some of its properties particularly its melt flow character, which is the major challenge in industrial application of starch due to its very high viscosity. Thermoplastic starch modification with tartaric acid during its thermal extrusion significantly reduced its melt flow character as well as its shear viscosity. This modification also improved the rheological characteristics such as shear viscosity, complex viscosity, storage modulus and loss modulus of blend compounds. Significant variation in melt flow characteristics of modified and unmodified TPS as well as blends was observed for all blend ratios as evidenced by ANOVA analysis with a p value being less than 0.05 at 95% confidence level. In another way, as TPS_TA content increased in the blends, shear viscosity, complex viscosity, storage modulus (G`) and loss modulus (G``) gets higher and also two crossover points were observed in the higher and lower angular frequencies as TPS_TA content increases but in blends with lower TPS_TA content and in neat PLA, loss modulus (G``) dominates at lower angular frequencies with a transition point coming at the end of the applied angular frequency range. In case of neat TPS_TA the storage modulus (G`) dominates over loss modulus (G``) throughout the entire range of angular frequency. The study also shows that the compatibilizer (PLA-g-MA) used during melt blending improved the properties of blends as can be seen from overall analysis and the melt spinnability study as successful melt spinning was achieved from compounds that are prepared from compatibilized blends. Structural analysis shows –OH peak shifting and peak intensity changes associated to tartaric acid modification and compatibilization of blends as evidenced by FTIR analysis. From the study it is evidenced that successful melt spinning of biopolymer fibers from the TPS/PLA blends, even with higher TPS contents 40%w/w and above is possible. The melt spun fibers have a diameter in a range of 12.0 – 124.0 µm and nice appearance with white color resembling cellulosic fibers. DSC analysis of melt spun fibers shows that the glass transition T_g shifted to higher values as take-up speed increases which is attributed to increased molecular orientation. In case of blends with higher TPS_TA content the T_g value gets higher and there is no shift in T_g value regardless of take-up speed which might indicate that higher contents of TPS_TA forms network structures and limits molecular chain mobility which in turn can raise the T_g value or it may indicate

the formation of more rigid amorphous TPS phase in the blend as a result of higher TPS_TA content. The T_m values show double melting peaks in the case of most of the melt spun fibers which might be attributed to the development of new forms of crystals as a result of process induced crystallization during fiber take-up. Tensile properties of melt spun fibers are relatively low as compared to neat PLA fibers, however they can be recommended for areas of applications that do not need more stress. The fibers can also give an advantage of biocompatibility and enhanced biodegradability.

ACKNOWLEDGEMENT

The authors of this research article would like to thank Leibniz-Institut für Polymerforschung (Dresden e. V.), Germany, for their cooperation on melt spinning trials and particularly Mr. Mathias Haeschel for his support. Additionally, the authors would like to thank Prof. Michael Rauch and Mrs. Susanne Schoedel from the Institut für Materialwissenschaften (ifm), Hof University for their cooperation on tensile test measurement.

RESEARCH FUNDING

This research received no external funding.

AUTHOR CONTRIBUTION

All authors have contributed to this paper. Selamu T.**:** Writing original draft, experimental work and data Analysis, Tamrat T: writing review and editing, Lucas G.: editing, visualization and supervision, Michael Nase: writing review, editing and supervision, Ines Kühnert: writing review and editing, Norbert Smolka: experimental work and editing.

CONFLICT OF INTEREST

The authors can declare that there is no conflict of interest.

DATA AVAILABILITY

The data sets generated during and/or analyzed during the current study are available from the corresponding author on reasonable request.

REFERENCES

[1] Naeimirad M, Krins B, Gruter GJM. A Review on Melt-Spun Biodegradable Fibers. Sustain 2023; 15(19). https://doi.org/10.3390/su151914474

[2] Chen X, Memon HA, Wang Y, Marriam I, Tebyetekerwa M. Circular Economy and Sustainability of the Clothing and Textile Industry. Mater Circ Econ 2021; 3(1): 1-9. https://doi.org/10.1007/s42824-021-00026-2

[3] Opperskalski TE, Sophia, Ridler TE, Sophie Joyce, Siew, SuetYin TE, Tan, Evonne T E. Preferred Fiber and Materials Market Report 2021; 118.

[4] Mehta S. Biodegradable textile polymers: a review of current scenario and future opportunities. Environ Technol Rev 2023; 12(1): 441-457. https://doi.org/10.1080/21622515.2023.2227391

[5] Tian W, *et al*. Recent progress in biobased synthetic textile fibers. Front Mater 2022; 1-12. https://doi.org/10.3389/fmats.2022.1098590

[6] Motloung MP, Mofokeng TG, Mokhena TC, Ray SS. Recent advances on melt-spun fibers from biodegradable polymers and their composites. Int Polym. Process 2022; 37(5): 523-540. https://doi.org/10.1515/ipp-2022-0023

[7] Syafiq RMO, *et al*. Corn starch nanocomposite films reinforced with nanocellulose 2024; 9(8): 2653-2681. https://doi.org/10.1515/psr-2022-0011

[8] Suja RN, Sridevi B, Thiagamani SMK. Mechanical and Dynamic Mechanical Characterization of Epoxy Composites Reinforced with Casuarina Leaf Bio Fibre. J Res Updat Polym Sci 2024; 13: 66-74. https://doi.org/10.6000/1929-5995.2024.13.08

[9] Samir A, Ashour FH, Hakim AAA, Bassyouni M. Recent advances in biodegradable polymers for sustainable applications. NPJ Mater Degrad 2022; 6(1). https://doi.org/10.1038/s41529-022-00277-7

[10] Cheng Y-L, *et al*. Starch: A Veritable Natural Polymer for Economic Revolution. Intech 2016; 11(tourism): p. 13. [Online]. Available: https://www.intechopen.com/books/advanced-biometric-technologies/liveness-detection-in-biometrics.

[11] Calambás Pulgarin HL, Caicedo C, López EF. Effect of surfactant content on rheological, thermal, morphological and surface properties of thermoplastic starch (TPS) and polylactic acid (PLA) blends. Heliyon 2022; 8(10). https://doi.org/10.1016/j.heliyon.2022.e10833

[12] Fonseca-Florido HA, et al. Effects of multiphase transitions and reactive extrusion on in situ thermoplasticization/ succination of cassava starch. Carbohydr Polym 2019; 225: 115250. https://doi.org/10.1016/j.carbpol.2019.115250

[13] Jullanun P, Yoksan R. Morphological characteristics and properties of TPS/PLA/cassava pulp biocomposites. Polym Test 2020; 88: 106522. https://doi.org/10.1016/j.polymertesting.2020.106522

[14] Temesgen S, Rennert M, Tesfaye T, Großmann L, Kuehnert I. Thermal, morphological , and structural characterization of starch-based bio-polymers for melt spinnability 2024; 1: 1-19. https://doi.org/10.1515/epoly-2024-0025

[15] Lendvai LDB. View of Mechanical, Morphological and Thermal Characterization of Compatibilized Poly(lactic acid)_Thermoplastic Starch Blends.pdf.

[16] Mittal V, Akhtar T, Matsko N. Mechanical, thermal, rheological and morphological properties of binary and ternary blends of PLA, TPS and PCL. Macromol Mater Eng 2015; 300(4): 423-435. https://doi.org/10.1002/mame.201400332

[17] Caicedo C, Pulgarin HLC. Study of the physical and mechanical properties of thermoplastic starch/poly(lactic acid) blends modified with acid agents. Processes 2021; 9(4). https://doi.org/10.3390/pr9040578

[18] Temesgen S, Rennert M, Tesfaye T, Nase M. Review on spinning of biopolymer fibers from starch. Polymers (Basel) 2021; 13(7): 1-24. https://doi.org/10.3390/polym13071121

[19] Joseph Arockiam A, *et al*. Mechanical and thermal characterization of additive manufactured fish scale powder

reinforced PLA biocomposites. Mater Res Express 2023; 10(7): 8-10.
https://doi.org/10.1088/2053-1591/ace41d

[20] Sriram M, Kadhirnilavan, Mohammed KAN, Anandhakumar S, Mishra A, Tiwari A. Bio-Based PLA Membranes for Ion Transport and Ion Filtration. J Res Updat Polym Sci 2023; 12: 220-230.
https://doi.org/10.6000/1929-5995.2023.12.21

[21] Mayekar PC, Limsukon W, Bher A, Auras R. Breaking It Down: How Thermoplastic Starch Enhances Poly(lactic acid) Biodegradation in Compost─A Comparative Analysis of Reactive Blends. ACS Sustain Chem Eng 2023; 11(26): 9729-9737.
https://doi.org/10.1021/acssuschemeng.3c01676

[22] Moghaddam MRA, Razavi SMA, Jahani Y. Effects of Compatibilizer and Thermoplastic Starch (TPS) Concentration on Morphological, Rheological, Tensile, Thermal and Moisture Sorption Properties of Plasticized Polylactic Acid/TPS Blends. J Polym Environ 2018; 26(8): 3202-3215.
https://doi.org/10.1007/s10924-018-1206-7

[23] Lendvai L, Brenn D. Mechanical, Morphological and Thermal Characterization of Compatibilized Poly(lactic acid)/Thermoplastic Starch Blends. Acta Tech Jaurinensis 2020; 13(1): 1-13.
https://doi.org/10.14513/actatechjaur.v13.n1.532

[24] Akrami M, Ghasemi I, Azizi H, Karrabi M, Seyedabadi M. A new approach in compatibilization of the poly(lactic acid)/thermoplastic starch (PLA/TPS) blends. Carbohydr. Polym 2016; 144: 254-262.
https://doi.org/10.1016/j.carbpol.2016.02.035

[25] Palai B, Biswal M, Mohanty S, Nayak SK. *In situ* reactive compatibilization of polylactic acid (PLA) and thermoplastic starch (TPS) blends; synthesis and evaluation of extrusion blown films thereof. Ind Crops Prod 2019; 141: 111748.
https://doi.org/10.1016/j.indcrop.2019.111748

[26] da Silva SC, Simões BM, Yamashita F, de Carvalho FA. Compatibilizers for biodegradable starch and poly (lactic acid) materials produced by thermoplastic injection. Res. Soc. Dev 2022; 11(14): e476111436521.
https://doi.org/10.33448/rsd-v11i14.36521

[27] Gunawardene OHP, *et al*. Compatibilization of starch/synthetic biodegradable polymer blends for packaging applications: A review. J Compos Sci 2021; 5(11): 1-33.
https://doi.org/10.3390/jcs5110300

[28] Ávila-Orta CA, Covarrubias-Gordillo CA, Fonseca-Florido HA, Melo-López L, Radillo-Ruíz R, Gutiérrez-Montiel E. PLA/modified-starch blends and their application for the fabrication of non-woven fabrics by melt-blowing. Elsevier - Carbohydrate Polymers 2023; 316: 120975.
https://doi.org/10.1016/j.carbpol.2023.120975

[29] Zarski A, Bajer K, Kapuśniak J. Review of the most important methods of improving the processing properties of starch toward non-food applications. Polymers (Basel) 2021; 13(5): 1-33.
https://doi.org/10.3390/polym13050832

[30] Fonseca-Florido HA, *et al*. Effects of multiphase transitions and reactive extrusion on in situ thermoplasticization/ succination of cassava starch. Carbohydr Polym 2019; 225.
https://doi.org/10.1016/j.carbpol.2019.115250

[31] Chen P, Xie F, Zhao L, Qiao Q, Liu X. Effect of acid hydrolysis on the multi-scale structure change of starch with different amylose content. Food Hydrocoll 2017; 69: 359-368.
https://doi.org/10.1016/j.foodhyd.2017.03.003

[32] Tupa MV, Altuna L, Herrera ML, Foresti ML. Preparation and Characterization of Modified Starches Obtained in Acetic Anhydride/Tartaric Acid Medium. Starch/Staerke 2020; 72(5-6): 1-11.
https://doi.org/10.1002/star.201900300

[33] Chauhan S, Raghu N, Raj A. Effect of maleic anhydride grafted polylactic acid concentration on mechanical and thermal properties of thermoplasticized starch filled polylactic acid blends. Polym Polym Compos 2021; 29(9_suppl): S400-S410.
https://doi.org/10.1177/09673911211004194

[34] Zhang C, Lan Q, Zhai T, Nie S, Luo J, Yan W. Melt crystallization behavior and crystalline morphology of Polylactide/Poly(ε-caprolactone) blends compatibilized by lactide-caprolactone copolymer. Polymers (Basel) 2018; 10(11).
https://doi.org/10.3390/polym10111181

[35] Zhang S, He Y, Yin Y, Jiang G. Fabrication of innovative thermoplastic starch bio-elastomer to achieve high toughness poly(butylene succinate) composites. Carbohydr Polym 2019; 206: 827-836.
https://doi.org/10.1016/j.carbpol.2018.11.036

[36] Oliver-Ortega H, Reixach R, Espinach FX, Méndez JA. Maleic Anhydride Polylactic Acid Coupling Agent Prepared from Solvent Reaction: Synthesis, Characterization and Composite Performance. Materials (Basel) 2022; 15(3).
https://doi.org/10.3390/ma15031161

[37] Hwang SW, Shim JK, Selke S, Soto-Valdez H, Rubino M, Auras R. Effect of maleic-anhydride grafting on the physical and mechanical properties of poly(L-lactic acid)/starch blends. Macromol Mater Eng 2013; 298(6): 624-633.
https://doi.org/10.1002/mame.201200111

[38] Rigolin TR, Costa LC, Venâncio T, Perlatti B, Bettini SHP. The effect of different peroxides on physical and chemical properties of poly(lactic acid) modified with maleic anhydride. Polymer (Guildf) 2019; 179.
https://doi.org/10.1016/j.polymer.2019.121669

[39] Ma P, Jiang L, Ye T, Dong W, Chen M. Melt free-radical grafting of maleic anhydride onto biodegradable poly(lactic acid) by using styrene as a comonomer. Polymers (Basel) 2014; 6(5): 1528-1543.
https://doi.org/10.3390/polym6051528

[40] Ramli H, Zainal NFA, Hess M, Chan CH. Basic principle and good practices of rheology for polymers for teachers and beginners. Chem Teach Int 2022; 4(4): 307-326.
https://doi.org/10.1515/cti-2022-0010

[41] Huneault MA, Li H. Morphology and properties of compatibilized polylactide/thermoplastic starch blends. Polymer (Guildf) 2007; 48(1): 270-280.
https://doi.org/10.1016/j.polymer.2006.11.023

[42] Rodriguez-Gonzalez FJ, Ramsay BA, Favis BD. Rheological and thermal properties of thermoplastic starch with high glycerol content. Carbohydr Polym 2004; 58(2): 139-147.
https://doi.org/10.1016/j.carbpol.2004.06.002

[43] Il Park D, Dong Y, Wang S, Lee SJ, Choi HJ. Rheological Characteristics of Starch-Based Biodegradable Blends. Polymers (Basel) 2023; 15(8).
https://doi.org/10.3390/polym15081953

[44] Ning W, Xingxiang Z, Na H, Jianming F. Effects of Water on the Properties of Thermoplastic Starch Poly(lactic acid) Blend Containing Citric Acid. J Thermoplast Compos Mater 2010; 23(1): 19-34.
https://doi.org/10.1177/0892705709096549

[45] Vlachopoulos J, Strutt D. Rheology of molten polymers. Multilayer Flex. Packag Technol Appl Food Pers Care Over-the-Counter Pharm Ind 2009; 57-72.
https://doi.org/10.1016/B978-0-8155-2021-4.10005-X

[46] Castro JM, *et al*. Thermoplastic starch/polyvinyl alcohol blends modification by citric acid-glycerol polyesters. Int J Biol Macromol 2023; 244.
https://doi.org/10.1016/j.ijbiomac.2023.125478

[47] Zhang S, He Y, Lin Z, Li J, Jiang G. Effects of tartaric acid contents on phase homogeneity, morphology and properties

of poly (butyleneadipate-co-terephthalate)/thermoplastic starch bio-composities. Polym Test 2019; 76: 385-395. https://doi.org/10.1016/j.polymertesting.2019.04.005

[48] Esmaeili M, Pircheraghi G, Bagheri R, Altstädt V. Poly(lactic acid)/coplasticized thermoplastic starch blend: Effect of plasticizer migration on rheological and mechanical properties. Polym Adv Technol 2019; 30(4): 839-851. https://doi.org/10.1002/pat.4517

[49] Bernreitner K, Neißl W, Gahleitner M. Correlation between molecular structure and rheological behaviour of polypropylene. Polym Test 1992; 11(2): 89-100. https://doi.org/10.1016/0142-9418(92)90040-I

[50] Strasser C. Polymer Rheology and Molecular Mass (Peek 1. pp. 2-5.

[51] Zeraatpishe M, Hassanajili S. Investigation of physical and rheological properties of LDPE/HDPE/thermoplastic starch biodegradable blend films. Polym Eng Sci 2023; 63(9): 3116-3134. https://doi.org/10.1002/pen.26432

[52] Trinh BM, Tadele DT, Mekonnen TH. Robust and high barrier thermoplastic starch - PLA blend films using starch-graft-poly(lactic acid) as a compatibilizer. Mater Adv 2022; 3(15): 6208-6221. https://doi.org/10.1039/D2MA00501H

[53] Galkina YA, Kryuchkova NA, Vershinin MA, Kolesov BA. Features of strong O-H···O and N-H···O hydrogen bond manifestation in vibrational spectra. J Struct Chem 2017; 58(5): 911-918. https://doi.org/10.1134/S0022476617050080

[54] Wang N, Yu J, Han C. Influence of citric acid on the properties of glycerol-plasticised cornstarch extrusion blends. Polym Polym Compos 2007; 15(7): 545-552. https://doi.org/10.1177/096739110701500704

[55] Esmaeili M, Pircheraghi G, Bagheri R. Optimizing the mechanical and physical properties of thermoplastic starch via tuning the molecular microstructure through co-plasticization by sorbitol and glycerol. Polym Int 2017; 66(6): 809-819. https://doi.org/10.1002/pi.5319

[56] Thiruganasambanthan T, Thiagamani SMK, Santulli C, Krishnasamy S, Muthukumar C. Preparation of Sodium Alginate/Rice starch blend polymer film for soil moisture sensing. Mater Today Proc 2022; 64: 352-356. https://doi.org/10.1016/j.matpr.2022.04.702

[57] Haryńska A, Janik H, Sienkiewicz M, Mikolaszek B, Kucińska-Lipka J. PLA-Potato Thermoplastic Starch Filament as a Sustainable Alternative to the Conventional PLA Filament: Processing, Characterization, and FFF 3D Printing. ACS Sustain. Chem Eng 2021; 9(20): 6923-6938. https://doi.org/10.1021/acssuschemeng.0c09413

[58] Jaderi Z, Tabatabaee Yazdi F, Mortazavi SA, Koocheki A. Effects of glycerol and sorbitol on a novel biodegradable edible film based on Malva sylvestris flower gum. Food Sci Nutr 2023; 11(2): 991-1000. https://doi.org/10.1002/fsn3.3134

[59] Tadmor Z, Costas GG. Principles of Polymer Process Ing Second Edition 2006.

[60] Li H, Huneault MA. Crystallization of PLA/Thermoplastic Starch Blends. Int Polym Process 2008; 23(5): 412-418. https://doi.org/10.3139/217.2185

[61] Yasuniwa M, Iura K, Dan Y. Melting behavior of poly(l-lactic acid): Effects of crystallization temperature and time. Polymer (Guildf) 2007; 48(18): 5398-5407. https://doi.org/10.1016/j.polymer.2007.07.012

[62] Yoksan R, Dang KM, Boontanimitr A, Chirachanchai S. Relationship between microstructure and performances of simultaneous biaxially stretched films based on thermoplastic starch and biodegradable polyesters. Int J Biol Macromol 2021; 190: 141-150. https://doi.org/10.1016/j.ijbiomac.2021.08.206

[63] Ziabicki A, Jarecki L, Sorrentino A. The role of flow-induced crystallisation in melt spinning. E-Polymers 2004; 072: 1-14. https://doi.org/10.1515/epoly.2004.4.1.823

[64] Richter LE, Carlos A, Beber DM. Influence of Take-up Speeds on the Structure, Properties and Dyeability of Novel Polyamide 5,6 As-spun Fibers.

[65] Müller P, *et al*. Interactions, structure and properties in PLA/plasticized starch blends. Polymer (Guildf) 2016; 103: 9-18. https://doi.org/10.1016/j.polymer.2016.09.031

[66] Ma X, Yu J, Kennedy JF. Studies on the properties of natural fibers-reinforced thermoplastic starch composites 2005; 62: 19-24. https://doi.org/10.1016/j.carbpol.2005.07.015

[67] Koike N, *et al*. Effects of melt-spinning speed on structure development of polypropylene fiber after necking. J Fiber Sci Technol 2020; 76(5): 161-169. https://doi.org/10.2115/fiberst.2020-0019

Received on 09-09-2024 Accepted on 02-10-2024 Published on 24-10-2024

https://doi.org/10.6000/1929-5995.2024.13.20